

Impact of changes in climate and CO₂ on the carbon storage potential of vegetation under limited water availability using SEIB-DGVM version 3.02

Shanlin Tong^{1,2,3}, Weiguang Wang^{2,3*}, Jie Chen^{1*}, Chong-Yu Xu⁴, Hisashi Sato⁵, Guoqing Wang⁶

¹State Key Laboratory of Water Resources and Hydropower Engineering Science, Wuhan University, Wuhan, 430072, Peoples R China

²State Key Laboratory of Hydrology-Water Resources and Hydraulic Engineering, Hohai University, Nanjing, 210098, Peoples R China

³College of Hydrology and Water Resources, Hohai University, Nanjing, 210098, Peoples R China

⁴Department of Geosciences, University of Oslo, Oslo, N-0316, Norway

⁵Japan Agency for Marine-Earth Science and Technology, Yokohama, 236-0001, Japan

⁶Nanjing Hydraulic Research Institute, Nanjing, 210029, Peoples R China

*Correspondence to: Weiguang Wang (wangweiguang2016@126.com); Jie Chen (jiechen@whu.edu.cn)

Abstract

Documenting year-to-year variations in carbon storage potential in terrestrial ecosystems is crucial for the determination of carbon dioxide (CO₂) emissions. However, the magnitude, pattern and inner biomass partitioning of carbon storage potential, and the effect of the changes in climate and CO₂ on inner carbon stocks, remain poorly quantified. Herein, we use a spatially explicit individual based-dynamic global vegetation model to investigate the influences of the changes in climate and CO₂ on the enhanced carbon storage potential of vegetation. The modelling included a series of factorial simulations using the CRU dataset from 1916 to 2015. The results show that CO₂ predominantly leads to a persistent and widespread increase in light-gathering vegetation biomass carbon stocks (LVBC) and water-gathering vegetation biomass carbon stocks (WVBC). Climate change appears to play a secondary role in carbon storage potential. Importantly, with the intensification of water stress, the magnitude of the light- and water-gathering responses in vegetation carbon stocks gradually decreases. Plants adjust carbon allocation to decrease the ratio between LVBC and WVBC for capturing more water. Changes in the pattern of vegetation carbon storage was linked to zonal limitations in water, which directly weakens and indirectly regulates the response of potential vegetation carbon stocks to a changing environment. Our findings differ from previous modelling evaluations of vegetation that ignored inner carbon dynamics and

32 demonstrates that the long-term trend in increased vegetation biomass carbon stocks is driven by CO₂
33 fertilization and temperature effects that are controlled by water limitations.

34 **1 Introduction**

35 As a result of the changes in climate and atmospheric carbon dioxide (CO₂), the terrestrial ecosystem
36 carbon cycle exhibits remarkable trends in interannual variations, which induce uncertainty in estimated
37 carbon budgets (Erb et al., 2018; Keenan et al., 2017). Recent studies assessing interannual fluctuations
38 in terrestrial carbon sinks have shown that the land carbon cycle is the most uncertain component of the
39 global carbon budget (Ahlstrom et al., 2015; Piao et al., 2020; Jung et al., 2017; Humphrey et al., 2018;
40 Gentine et al., 2019; Humphrey et al., 2021). These uncertainties result from an incomplete understanding
41 of vegetation biomass carbon production, allocation, storage, loss, and turnover time (Bloom et al., 2016).
42 The extent and distribution of vegetation carbon storage is central to our understanding of how to
43 maintain a balanced land carbon cycle. Changes in terrestrial vegetation carbon storage have a significant
44 effect on atmospheric CO₂ concentrations and determine whether biomes become a source or sink of
45 carbon (Erb et al., 2018; Humphrey et al., 2018; Terrer et al., 2021). Therefore, investigating the
46 processes producing changes in carbon storage is key to improving the accuracy of estimated terrestrial
47 carbon budgets, and to tap the greenhouse-gas moderation potentials of vegetation (Ipcc, 2007; Roy et
48 al., 2001).

49

50 The atmospheric CO₂ concentration is affected by the vegetation carbon stock, while the long-term trend
51 of vegetation carbon storage capacity is also affected by the changes in climate and CO₂. Since the
52 beginning of industrialization, there has been a noticeable enhancement in the plant capacity of storing
53 and sequestering carbon, which is needed for stabilizing greenhouse gas concentrations and mitigating
54 global warming (Chen et al., 2019; Pan et al., 2011; Le Noë et al., 2020; Magerl et al., 2019; Bayer et al.,
55 2015; Harper et al., 2018). Due to the interaction between terrestrial vegetation and a changing
56 environment, both photosynthesis and respiration of the vegetation also changed. To better absorb CO₂
57 and sunlight required for photosynthesis, vegetated zones are gradually covered by vegetation with
58 higher plant height and wider leaf area (Erb et al., 2008). This change has coincided with a widespread
59 change in other vegetation features, including a positive increase in annual gross primary productivity

60 and a greening of the biosphere (Madani et al., 2020; Zhu et al., 2016). The spatiotemporal distribution
61 and environmental drivers in total carbon storage potential have been well documented on the basis of
62 model estimates and satellite-based assessments (Erb et al., 2007; Erb et al., 2018; Bazilevich et al., 1971;
63 Saugier et al., 2001; Bartholome and Belward, 2005; Olson et al., 1983; Pan et al., 2013; Ajtay et al.,
64 1979; Ruesch and Gibbs, 2008; Kaplan et al., 2011; Shevliakova et al., 2009; Prentice et al., 2011; West
65 et al., 2010; Hurtt et al., 2011). In contrast, the variability of inner components of carbon storage potential
66 has not been extensively studied. Without an accurate assessment of the dynamics of each fraction,
67 attribution of carbon storage potential to environmental drivers is highly uncertain. Consequently,
68 partitioning potential vegetation carbon storage and revealing its inner processes are essential to
69 accurately comprehend the current state of carbon storage capacity and reveal the influence of various
70 drivers on the long-term trend of carbon storage potential.

71

72 The change of carbon storages in vegetation inner components is not only affected by environmental
73 factors, but also controlled by allocation scheme of assimilated carbon. Fractional dynamics of the carbon
74 stock are widely used as a key indicator to investigate the responses of vegetation to environmental
75 drivers, which also reflect the response strategies of vegetation in environments with different water
76 limitations (Yang et al., 2010). In arid regions, vegetation utilizes a tolerance strategy to allocate biomass,
77 storing more biomass carbon in roots to resist enhanced water stress (Chen et al., 2013). Conforming to
78 the optimal partitioning hypothesis, plants store more carbon in shoots and leaves in environments where
79 water is more available and shift more carbon to roots when water is more limited (Yang et al., 2010;
80 McConnaughay and Coleman, 1999). Water availability controls both carbon allocation and storage and
81 can potentially transform zones characterized by a positive response to changes in climate and CO₂ to
82 zones exhibiting a negative response. For example, global warming positively stimulates plant
83 productivity (Keenan et al. 2017), while Madani et al. (2020) found that ~~plants productively with water~~
84 ~~stress show a negative response to temperature rise in tropical zones~~ productively showed a negative
85 response to temperature in tropical zones due to increasing water stress. With increased warming, water
86 limitations are predicted to increasingly reduce the proportion of leaves' biomass, and decrease plant
87 photosynthesis (Ma et al., 2021). Water limitations have a strong regulating effect on the spatial pattern
88 of change in vegetation carbon storage, demonstrating the effects of the changes in climate and CO₂ on

89 the dynamics of the plant organs are affected by the terrestrial water gradient. Thus, it is important to
90 systematically investigate the distinct responses of carbon storage potential to changes in climate and
91 CO₂ under differing conditions of water stress.

92

93 As documented above, many studies have investigated the total changes in zonal and global terrestrial
94 storage of carbon, while few studies have examined trends in the components partitioning of vegetation
95 carbon storage. Large gaps in our knowledge of the effects of various drivers on the partitioning of carbon
96 stocks in vegetation biomass remain. Meanwhile, plants adjust carbon allocation scheme to adapt to
97 environmental change. With increased warming, an increase in the magnitude of water stress may
98 dramatically change or even reverse the impact of these drivers on inner components of carbon storage
99 (Ma et al., 2021). Evaluating the response pattern of carbon stocks to various drivers under conditions of
100 limited water is elemental for clearly documenting the response mechanism of vegetation carbon storage
101 potential.

102

103 Here, we use a spatially explicit individual-based dynamic global vegetation model (SEIB-DGVM),
104 along with the components partitioning method to (1) systematically determine the long-term variability
105 of carbon storage potential and understand its response mechanisms, and (2) estimate trends in
106 partitioning of potential biomass carbon stocks of vegetation biomass. Throughout this study, the
107 potential biomass carbon stock, biomass carbon stored in vegetation without anthropogenic disturbance,
108 is recognized as an indicator of the potential of carbon storage by natural vegetation. Using a set of
109 factorial simulations to isolate responses to environmental change, we analyse the contributions of
110 multiple driving factors to the trends of two fractions of carbon stock at large scales individually. We
111 then conceptualize the role of water availability through an aridity index (AI), in which hydrological
112 zones are subdivided by their degree of aridity. By comparing the differences in the magnitude of
113 response between the fractions of light- and water-gathering carbon stocks for varying degrees of water
114 availability, we assess the effect of water limitations on the response pattern of potential carbon stocks
115 to changes in climate and CO₂.

116 **2 Model description, experimental design, observational data, and evaluation metrics**

117 In this section, we provided a list of data source (Sect. 2.1), an overview of the modelling concept (Sect.
118 2.2), the representation of biomass carbon stock partitioning in the SEIB-DGVM (Sect. 2.3), an overview
119 of the experimental scheme used in the model simulations (Sect. 2.4), and an overview about data source
120 and pre-processing of observation dataset for model evaluation (Sect. 2.5).

121 **2.1 Forcing Data**

122 Long-term daily meteorological time-series data are required to run model simulations, including
123 precipitation, daily range of air temperature, mean daily air temperature, downward shortwave radiation
124 at midday, downward longwave radiation at midday, wind velocity, and relative humidity. These data
125 were obtained from the Climatic Research Unit (CRU) time series 4.00 gridded dataset (degree 0.5°) for
126 the period 1901–2015 (Harris et al., 2020). Because the CRU dataset is a monthly based dataset, the
127 monthly meteorological data were converted into daily climatic variables by supplementing daily
128 climatic variability within each month using the National Centre for Environmental Prediction (NCEP)
129 daily climate dataset. The NCEP data, displayed using the T62 Gaussian grid with 192×94 points, was
130 interpolated into a 0.5° grid (which corresponds to the CRU dataset) using a linearly interpolation method.
131 By combining the CRU data, with the interpolated NCEP dataset, we were able to directly obtain the
132 most of driving meteorological data (details in Sato et al. (2020)). Neither the CRU nor NCEP datasets
133 included downward shortwave and longwave radiation at midday. Thus, daily cloudiness values in the
134 NCEP were used to calculate radiation values using empirical functions (Sato et al., 2007). These data
135 were all aggregated to a daily timescale with 0.5° resolution to run SEIB-DGVM.

136

137 Atmospheric CO_2 concentrations were collected from Sato et al. (2020), which contains reconstructed
138 CO_2 concentrations between 1901 and 2015. The statistical reconstruction of global atmospheric CO_2
139 was used in this analysis. These reconstructions were based on present annual CO_2 concentrations
140 recorded from the Mauna Loa monitoring station. These data assume atmospheric CO_2 concentration
141 was 284 ppm in 1750, and statistically interpolates atmospheric CO_2 concentrations to fill the gap from
142 1750 to 2015.

143

144 The physical parameters of the soil used in the model include soil moisture at the saturation point, field
145 capacity, matrix potential, wilting point and albedo. These data were obtained from the Global Soil
146 Wetness Project 2.

147 **2.2 Overview of modelling concept in SEIB-DGVM**

148 Model SEIB-DGVM version 3.02 (Sato et al., 2020) was employed in this study. This is a process-based
149 dynamic global vegetation model driven by meteorological and soil data. It is an explicit and
150 computationally efficient carbon cycle model designed to simulate transient effects of environmental
151 change on terrestrial ecosystems and land-atmosphere interactions. It describes three groups of processes:
152 land-based physical processes (e.g., hydrology, radiation, aridity), plant physiological processes (e.g.,
153 photosynthesis, respiration, litter), and plant dynamic processes (e.g., establishment, growth, mortality).
154 Twelve plant functional types (PFTs) were classified. During the simulation, a sample plot was
155 established at each grid ~~box~~cell, and then the growth, competition, and mortality of each the individual
156 PFTs within each plot were modelled by considering the specify conditions for that individual as it relates
157 to other individuals that surround it (Sato et al., 2007).

158

159 SEIB-DGVM treats the relationships between soil, atmosphere, and terrestrial biomes in a consistent
160 manner, including the fluxes of energy, water, and carbon. Based on specified climatic conditions and
161 soil properties, SEIB-DGVM simulates the carbon cycle, energy balance, and hydrological processes.
162 SEIB-DGVM utilizes three computational time steps: (1) During the growth phase, the metabolic
163 procedures including photosynthesis, respiration, and carbon allocation are executed for each individual
164 tree every simulation day. (2) The monthly process of tree growth including reproduction, trunk growth,
165 and expansion of a cross-sectional area of the crown are executed. (3) On the last day of each year, the
166 height of the lowest branch increases as a result of purging crown disks, or ~~self-pruning~~self-pruning
167 branches, at the bottom of the crown layer. The simulated unit of the model is a 30 m × 30 m spatially
168 explicit ‘virtual forest’. A grass layer was placed under the woody layer, and provides for a
169 comprehensive, spatially explicit quantification of terrestrial carbon sinks and sources. The soil depth
170 was set at 2 m and was divided into 20 layers, each with a thickness of 0.1 m. The photosynthetic rate of
171 a single-leaf was simulated following a Michaelis-type function (Ryan, 1991). Respiration was divided
172 into two types: growth respiration and maintenance respiration. Growth respiration is defined as a

173 construction cost for plant biosynthesis, which is quantified by the chemical composition of each organ
174 (Poorter, 1994). Maintenance respiration of live plants occurs every day regardless of the phenological
175 phase, and is controlled by the temperature and nitrate content of each organ (Ryan, 1991). For a wide
176 variety of plant organs, the maintenance respiration rate is linearly related to the nitrogen content of
177 living tissue. The relative proportions of nitrogen in each organ for any PFT are linearly correlated. N-
178 deposition isn't included in SEIB-DGVM. Atmospheric CO₂ was envisioned to be absorbed by
179 photosynthesis of woody PFTs and grass PFTs. This assimilated carbon flux was then allocated into all
180 the plant organs (leaf, trunk, root, and stock), where maintenance respiration and growth respiration occur.
181 The hydrology module treats precipitation, canopy interception, transpiration, evaporation, meltwater,
182 and penetration.

183 **2.3 Carbon stock of vegetation biomass partitioning**

184 **2.3.1 Parameterization of daily allocation**

185 Flexible allocation schemes about resources and biomass are set up in the framework of the SEIB-DGVM
186 biogeochemical model. Based on the updated observation data, the allocation schemes of Boreal Needle-
187 leaved summer-green trees and Tropical Broad-leaved evergreen trees are improved at SEIB-DGVM
188 V3.02. Allocation schemes of other PFTs are the same as the original version. Atmospheric CO₂ is
189 assimilated by the photosynthesis of both woody and grass foliage, and then is added into the non-
190 structural carbon of the plant. This non-structural carbon of photosynthetic production is allocated to all
191 the plant organs (foliage, trunk, root, and stock), supplying what is needed for the maintenance and
192 growth of each organ. When the non-structural carbon is greater than 0 during the growth phase, the
193 following dynamic carbon allocation is executed for each individual plant at the daily time scale, such
194 that:

195 (1) When the fine root biomass ($mass_{root}$) of wood or grass does not satisfy minimum requirements for
196 fulfilling functional balance ($mass_{leaf}/FR_{ratio}$), the mass of non-structural carbon is allocated to the root
197 biomass to supplement the deficit. Here, $mass_{leaf}$ is the leaf biomass, and FR_{ratio} is the ratio of $mass_{leaf}$ to
198 $mass_{root}$ satisfying the functional balance.

199 (2) The stock biomass is supplemented until it is equal to leaf biomass. This scheme is active after the
200 first thirty days of the growing phase.

201 (3) Woody leaf biomass is constrained by three limitations of the maximum leaf biomass, which are
 202 calculated as follows:

$$203 \quad max_1 = (crown_{area} + \pi crown_{diameter} crown_{depth}) \frac{LA_{max}}{SLA} \quad (1)$$

$$204 \quad max_2 = ALM_1 \frac{\pi(dbh_{heartwood}/2 + dbh_{sapwood}/2)^2 - \pi(dbg_{heartwood}/2)^2}{SLA} \quad (2)$$

$$205 \quad max_3 = \frac{mass_{available}}{RG_f} \quad (3)$$

$$206 \quad mass_{leaf} = \min(max_1, max_2, max_3) \quad (4)$$

207 where max_1 , max_2 , and max_3 are, respectively, maximum leaf biomass for a given crown surface
 208 area, cross-sectional area of sapwood, and non-structural carbon; SLA is a constant of PFTs leaf area
 209 ($m^2 g^{-1}$); LA_{max} is the plant functional type specific maximum leaf area per unit crown surface area
 210 excluding the bottom layer ($m^2 m^{-2}$); ALM_1 represents the area of transport tissue per unit biomass, and
 211 is a constant (dimensionless). If the $mass_{leaf}$ is less than the minimum (max_1, max_2, max_3), the mass of
 212 non-structural carbon is allocated into leaf biomass to supplement the deficit.

213 When the leaf area index of grass equals the optimal leaf area index, it stops to allocate non-structural
 214 carbon to grass leaf, which is calculated as:

$$215 \quad lai_{opt} = \frac{\ln par_{grass} - \ln \left\{ \frac{p_{sat}}{lue} \left[\left(1 - \frac{cost/SLA}{0.09093 \times dlen \times p_{sat}} \right)^{-2} - 1 \right] \right\}}{eK} \quad (5)$$

216 where lai_{opt} is the optimal leaf area index ($m^2 m^{-2}$); par_{grass} is the grass photosynthetically active
 217 radiation ($\mu mol \text{ photon } m^{-2} s^{-1}$); p_{sat} is the light-saturated photosynthetic rate ($\mu CO_2 m^{-2} s^{-1}$); lue is
 218 the light-use efficiency of photosynthesis ($mol CO_2 mol \text{ photon}^{-1}$); $cost$ is the cost of maintaining
 219 leaves per unit leaf mass per day ($g DM g DM^{-1} day^{-1}$); $dlen$ is day length (hour); and eK is light
 220 attenuation coefficient at midday.

221 (4) When non-structural carbon is less than 10 g dry mass (DM) PFT⁻¹ or annual NPP is less than 10 g
 222 DM PFT⁻¹ in the previous year, the following daily simulation processes (5-6) will be skipped.

223 (5) When total woody biomass is more than 10 kg DM, which defines the minimum tree size for
 224 reproduction, 10% of non-structural carbon is used for every daily process of reproduction, including
 225 having flowers, pollen, nectar, fruits, and seeds. These organs are not explicitly modelled in SEIB-
 226 DGVM.

227 (6) During the simulation of trunk growth, the remaining non-structural carbon is allocated to sapwood
 228 biomass. There is no direct allocation to heartwood, which is transformed slowly from sapwood biomass.

229 For grass PFTs biomass, the densities of all organs comprising the biomass never decline below 0.1 g
 230 DM m⁻² even if the environment is deteriorated for grass survival. A more detailed description of SEIB-
 231 DGVM is given by Sato et al. (2007).

232

233 To control plant phenology and the rate of photosynthesis as a function of the limitation in terrestrial
 234 water, the physiological status of the limitation of terrestrial water is calculated as:

$$235 \quad p_{sat} = PMAX ce_{tmp} ce_{co_2} ce_{water} \quad (6)$$

$$236 \quad ce_{water} = \sqrt{stat_{water}} \quad (7)$$

$$237 \quad stat_{water} = \frac{\max(pool_{w(1)}/Depth_{(1)}, pool_{w(2)}/Depth_{(2)}) - W_{wilt}}{W_{fi} - W_{wilt}} \quad (8)$$

238 where p_{sat} is the single-leaf photosynthetic rate of tree PFTs and grass PFTs ($\mu\text{mol CO}_2 \text{ m}^{-2} \text{ s}^{-1}$);
 239 $PMAX$ is the potential maximum of photosynthetic rate ($\mu\text{mol mol}^{-1} \text{ CO}_2 \text{ m}^{-2} \text{ s}^{-1}$); ce_{tmp} and ce_{co_2} are
 240 the temperature and CO₂ concentration effect coefficient (dimensionless), separately; ce_{water} is the
 241 water effect coefficient (dimensionless); $stat_{water}$ is the physiological status of the terrestrial water
 242 limitation, which ranges between 0.0–1.0, dimensionless; $pool_{w(n)}$ is the water content in soil layer n,
 243 mm; $Depth_{(n)}$ is the depth of the soil layer n, mm; W_{wilt} is soil moisture at the wilting point, m⁻¹;
 244 and W_{fi} is soil moisture at field capacity, m⁻¹. When the temperature of all soil layers is less than 0°
 245 C, $stat_{water}$ is equal to 0.

246 **2.3.2 Carbon stock partitioning method**

247 SEIB-DGVM allocates and stores the biomass carbon in four pools of woody PFT (foliage, trunk, root,
 248 and stock) and three pools of grass PFT (foliage, root, and stock). To investigate the fractional variability
 249 of carbon sequestration potential between the pools, we partitioned potential vegetation carbon stocks
 250 based on the physiological function of the plant (Figure A1). The root-shoot ratio (R/S) has been used to
 251 distinguish and investigate the ratio of below-ground biomass (root biomass) and above-ground biomass
 252 (shoot biomass) (Zhang et al., 2016). In this study, we adjusted the method of calculating the R/S ratio
 253 by distinguishing between the light-gathering vegetation biomass carbon stock (LVBC) and the water-
 254 gathering vegetation biomass carbon stock (WVBC). LVBC represents the biomass carbon invested by
 255 plant is used to gather sunlight, including biomass carbon from woody foliage, woody trunk, and grass
 256 foliage. WVBC represents biomass carbon used to gather water, including biomass carbon from woody

257 fine roots and grass fine roots, excluding the stock pool. Stock biomass is used for foliation after dormant
 258 phase and after fires, which is reserve resource in each individual tree. Fine root biomass is just a tiny
 259 fraction to the total biomass, but it has a very high turnover rate and determines the capacity of vegetation
 260 to absorb soil water. Thus,

$$261 \frac{LVBC}{WVBC} = \frac{Tmass_{leaf} + Tmass_{trunk} + Gmass_{leaf}}{Tmass_{root} + Gmass_{root}} \times 100\% \quad (9)$$

262 where *LVBC* is light-gathering vegetation biomass carbon stock (kg C m⁻²); *WVBC* is water-gathering
 263 vegetation biomass carbon stock (kg C m⁻²); *Tmass_{leaf}* is the leaf biomass carbon stock of woody
 264 vegetation (kg C m⁻²); and *Tmass_{trunk}* is the trunk biomass carbon stock of trees (kg C m⁻²), including
 265 both branch and structural roots. This biomass is simplistically attributed to light-gathering vegetation
 266 organs and is used primarily to support the plant. *Gmass_{leaf}* is the leaf biomass carbon stock of grass
 267 (kg C m⁻²); whereas *Tmass_{root}* and *Gmass_{root}* are functional root (fine roots) biomass carbon stocks
 268 of trees and grass, separately (kg C m⁻²), which absorb water and nutrition from soil.

269 2.4 Experimental design

270 2.4.1 Setup of model runs

271 SEIB-DGVM simulations begin with seeds of selected PFTs planted in bare ground. The establishment
 272 of PFTs seeds are determined by the climatic conditions in each grid cell. We inputted the transient
 273 climate data from 1901 to 1915 to spin up the model in a repetitive loop. No obvious trend in climatic
 274 factors was observed during this period (Tei et al., 2017). A spin-up period of 1050 years was necessary
 275 to bring the terrestrial vegetation carbon cycle into a dynamic equilibrium. To reach quasi-equilibrium
 276 in the vegetation biomass, about 1000 years of simulation was required as a spin-up procedure.

277 2.4.2 Factorial simulation scheme

Table 1. List of factorial simulations used in this study

Factorial simulation	CO ₂ concentration	Precipitation	Temperature	Radiation	Other drivers
S1	√	√	√	√	√
S2	√				
S3	√	√			
S4	√		√		
S5	√			√	
S6	√				√

Note: In factorial simulation S1, historical atmospheric CO₂ concentration and historical climate fields from the CRU data set were used. In simulation S2, only historical atmospheric CO₂ concentration was used, and climate variables of the transient period (1901–1915) were repeatedly input. In simulation S3 (or S4, S5), only historical atmospheric CO₂ concentrations and precipitation (or temperature, radiation) were input, and climate variables of the transient period (1901–1915) were repeatedly input. In the last simulation S6, only historical atmospheric CO₂ concentrations and other climate variables were input, including wind velocity and relative humidity.

278 In order to further quantify the relative contributions of varying atmospheric CO₂ concentrations,
279 precipitation, temperature, radiation, and other factors (wind velocity and relative humidity), we
280 performed six factorial simulations. In simulation S1, atmospheric CO₂ concentration and all of climate
281 variables were varied. In simulation S2, only atmospheric CO₂ concentration was varied, and climate
282 variables were held constant (Climate variables of the transient period (1901-1915) were repeatedly
283 inputted). In simulation S3 (or S4, S5), atmospheric CO₂ and precipitation (or temperature, radiation)
284 were varied, and other climate variables were held constant. In simulation S6, atmospheric CO₂, wind
285 velocity, and relative humidity were varied, and other climate variables were held constant. Finally, S2
286 was used to evaluate the effects of CO₂ fertilization on carbon stock variation. The differences of S2-S3,
287 S2-S4, S2-S5, and S2-S6 were used to evaluate the response of carbon stock growth to precipitation,
288 temperature, radiation, and other drivers, respectively.

289 **2.4.3 Non-parametric test methods**

290 Each driving factor (atmosphere CO₂, precipitation, temperature, and radiation) has a different influence
291 on the carbon stock, so it is difficult to make a simple pre-assumption about the population distribution
292 pattern for factorial simulations. We used the non-parametric Mann-Kendall and Sen's slope estimator
293 statistical tests (Gocic and Trajkovic, 2013) to assess the ability of SEIB-DGVM to simulate the response
294 patterns of carbon storage potential to a change in climate and CO₂ concentrations. We regressed the
295 simulated hundred-year mean global average carbon stock time series to reveal the accumulative
296 influences of the single variables based on the factorial simulations where only one or two drivers were
297 varied. As shown in Figures A2 and A3, detection trends of LVBC and WVBC for all driving factors
298 performed statistically well (in agreement at the 95% confidence intervals), indicating this analytical
299 method was suitable for trend attribution at the global scale.

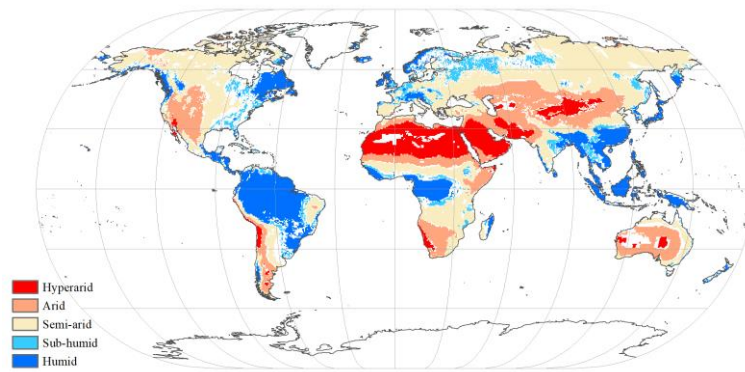


Figure 1. Global spatial patterns of water availability. Spatial variations in water availability were categorized based on the multiyear average aridity index (AI), defined as the ratio of the multiyear mean precipitation to the potential evapotranspiration. Categories include: hyper-arid ($AI \leq 0.05$), arid ($0.05 < AI \leq 0.2$), semi-arid ($0.2 < AI \leq 0.5$), sub-humid ($0.5 < AI \leq 0.65$), and humid ($AI > 0.65$).

The white grid cell was not assigned hydrological category.

301 Locally available water strongly regulates and limits the response of carbon stocks to changes in climate
 302 and CO₂. We used aridity index (AI) to distinguish between the global hydrological regions for
 303 comparing the long-term trend in carbon stocks over different hydrological environments, and for
 304 quantifying the influences of each hydrological environment on the variations in the trends. The AI was
 305 defined as:

$$306 \quad AI = \frac{\bar{P}}{\overline{ET_p}} \quad (10)$$

307 where \bar{P} is the multiyear mean precipitation (mm year⁻¹); and $\overline{ET_p}$ is the multiyear mean potential
 308 evapotranspiration (mm year⁻¹), which was calculated by the Penman-Monteith model (Monteith and
 309 Unsworth, 1990). As in a previous study (Chen et al., 2019), five hydrological regions were categorized
 310 based on a AI value. Under the influences of climate change, the hydrological condition was changed in
 311 some grid cells (Figure A4). For example, the grid cell classified as sub-humid zone in the period of
 312 1916-1945 was redefined as semi-arid zone in the period of 1986-2015. In this study, grid cells with
 313 consistent hydrological condition between the period of 1916-1945 and the period of 1986-2015 were
 314 selected and classified (Figure 1).

315 **2.5 Observation dataset for model evaluation**

316 A global time series of potential vegetation carbon was modelled by the SEIB-DGVM between 1916-
317 2015. In terrestrial vegetation biomes, there is a high correlation between biomass carbon stock density
318 and NPP per unit (Erb et al., 2016; Kindermann et al., 2008) (Figure A1). Thus, we collected NPP
319 observation dataset and used NPP as a proxy of the carbon stock to assess model accuracy. Ecosystem
320 Model-Data Intercomparison (EMDI) builds upon the accomplishments of the original worldwide
321 synthesis of NPP measurements and associated model driver data prepared by Global Primary Production
322 Data Initiative. We obtained the monitoring station data from the EMDI working group, and then
323 compared their data with modelled multiyear average NPP in the period of 1916-1999 (Figure 2).

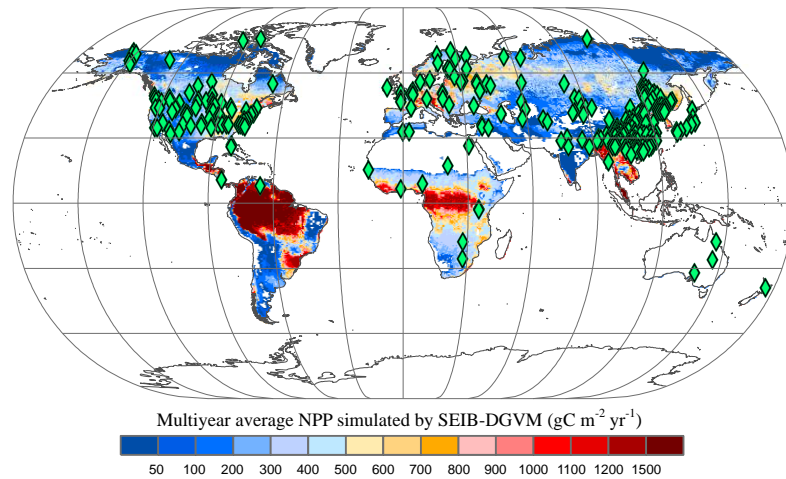


Figure 2. Multiyear average NPP simulated by SEIB-DGVM and EMDI global site distribution.

Green rhombuses indicate the monitoring stations of the EMDI.

324 However, *in-situ* observations are sparse for global spatial-temporal validation. Therefore, we used the
325 MOD17A3 products to further verify the simulated potential NPP in the twenty first century. These data
326 were collected by the Moderate Resolution Imaging Spectroradiometer and are some of the most widely
327 used data to assess the accuracy of global model simulations (Gulbeyaz et al., 2018). The natural
328 vegetation zones refer to the hypothetical condition that would prevail in an assumed absence of
329 anthropogenic activity, but under historical climate fields (Erb et al., 2018; Haberl et al., 2014). The
330 potential NPP is defined as that assimilated carbon stored in natural vegetation without the disturbance
331 of anthropogenic activities (Erb et al., 2018).

332

333 In order to distinguish the distribution of vegetation ~~zones~~ grid cells without anthropogenic disturbance,

334 we obtained global land cover types in the period 2001-2015 from MCD12C1 (Table A1). We included
335 grid cells whose largest vegetation component ~~defined vegetation grid cells as those whose largest~~
336 ~~component~~ was evergreen needleleaf forest, evergreen broadleaf forest, deciduous needleleaf forest,
337 deciduous broadleaf forest, mixed forest, closed shrublands, open shrublands, woody savannas, savannas
338 or grasslands. Other grid cells were excluded from our analysis.

339

340 Part of grid cells covered by grassland were grazed by livestock, leading to the decrease of NPP of grass
341 PFTs. There is a weak anthropogenic disturbance in rangeland, while managed pasture is intensely grazed
342 by livestock. To remove pasture area with strong anthropogenic disturbance. ~~We~~ ~~we~~ obtained land-use
343 forcing data from Land-Use Harmonization (LUH2) to map the distribution of managed pasture data
344 from 2001 to 2015 (Hurt et al., 2020). As shown in Figure A5, grassland in eastern Asia, western Europe,
345 south central Africa, and western South America were severely affected by grazing. For exhibit the
346 disturbance of managed pasture, we calculated the mean fraction of managed pasture within the
347 corresponding 0.5° grid unit. When the fraction of managed pasture over 10%, the grid cell was
348 considered to be affected by managed pasture. To reduce the interference effects of livestock grazing,
349 we first removed the grid cells ~~–~~ affected by managed pasture. Then, we map the distribution of natural
350 vegetation ~~zones~~ grid cells without anthropogenic disturbance (Figure A6). ~~We declare that~~ ~~†~~ This
351 exclusion method is only used for potential NPP comparison.

352 **3 Results and discussion**

353 **3.1 Evaluation of SEIB-DGVM**

354 Figure 3 illustrates the comparison between model simulated and observed multi-year mean NPP during
355 1916-1999. The determined coefficient (R^2) between EMDI observed and estimated multiyear average
356 NPP of 669 *in-situ* observations is 0.54, which is significant at the $p=0.01$ level. The slope of the
357 regressed line is 0.70 during the twentieth century.

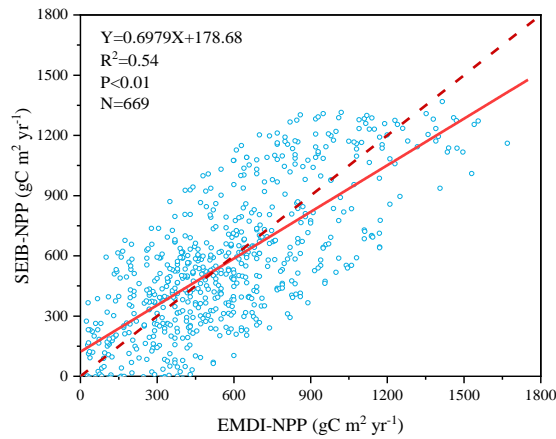


Figure 3. Comparison of multiyear average NPP calculated by SEIB-DGVM and EMDI for the twentieth century. The solid line is the best fit curve; and the dashed line represents a perfect correspondence in the results of the two.

358 Based on land cover types dataset from 2001 to 2015, we obtained NPP-MOD17A3 data in natural
 359 vegetation zones without anthropogenic disturbance at the same period. Figure 4 shows that the modelled
 360 NPP from the SEIB-DGVM exhibited a high degree of consistency with the NPP-MOD17A3 data in
 361 natural vegetation zones over the period ($R^2=0.63$, $p<0.05$). The general spatiotemporal agreement
 362 between the simulated NPP derived from SEIB-DGVM with *in-situ* observations and derived from
 363 satellites reveals that it is reasonable to use the SEIB-DGVM simulations to evaluate the same
 364 mechanisms controlling global potential biomass carbon stocks of vegetation.

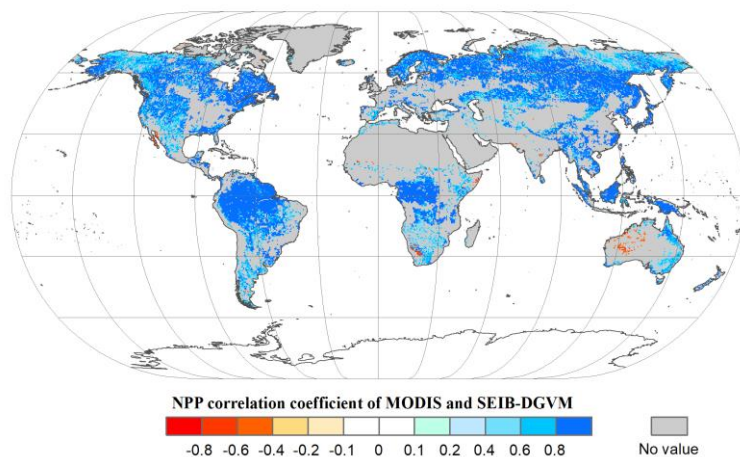


Figure 4. Spatial patterns in the potential NPP correlation coefficients ($P<0.05$) between SEIB-DGVM and MODIS between 2001–2015. These data were used to validate SEIB-DGVM.

365 Finally, the modelled result of potential vegetation biomass carbon stock was compared with current

366 existing data from the literature and state-of-the-art datasets. Figure 5 shows that the modelled results are
 367 within the range of potential carbon stocks, which indicate that the SEIB-DGVM reliably simulated the
 368 carbon stock dynamics.

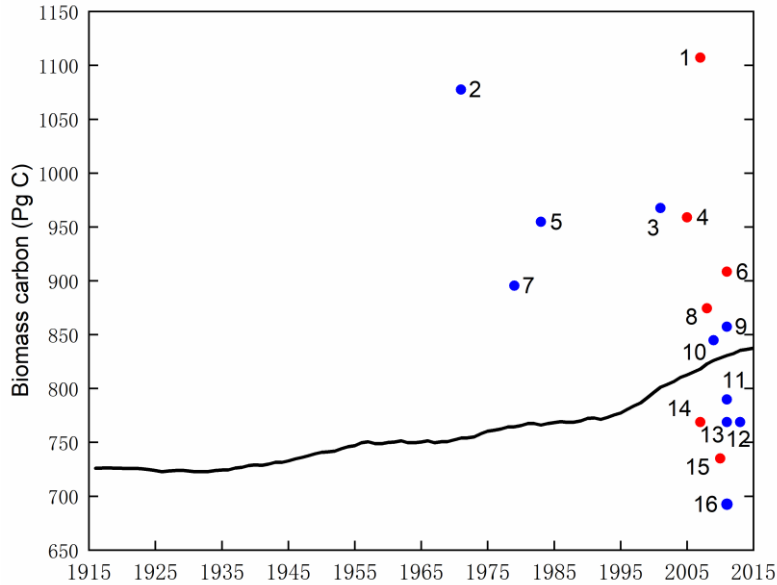


Figure 5. Estimates of the potential vegetation biomass carbon stock from the literature (blue plot), state-of-the-art datasets (red plot) and this study (black line). Datasets are from the following studies: (1)(Erb et al., 2018; Erb et al., 2007), (2)(Bazilevich et al., 1971), (3)(Saugier et al., 2001), (4)(Erb et al., 2018; Bartholome and Belward, 2005), (5)(Olson et al., 1983), (6)(Erb et al., 2018; Pan et al., 2011), (7)(Ajtay et al., 1979), (8)Erb et al., 2018; Ruesch and Gibbs, 2008), (9)(Kaplan et al., 2011), (10)(Shevliakova et al., 2009), (11)(Kaplan et al., 2011), (12)(Pan et al., 2013), (13)(Prentice et al., 2011), (14)(Erb et al., 2018; Erb et al., 2007), (15)(Erb et al., 2018; West et al., 2010), (16)(Hurt et al., 2011).

369 3.2 Enhanced carbon stocks and its fractions

370 We distinguished the changes of LVBC and WVBC from total vegetation carbon stocks. The historical
 371 temporal trends over the period are ~~showed~~ shown in Figure 6a. The potential vegetation carbon stock
 372 exhibits a net increase of 119.26 ± 2.44 Pg C in the last century (± 2.44 represents intra-annual fluctuation
 373 in carbon stock, which is the difference between maximum value and minimum value of carbon stock
 374 within the year). Based on Pearson correlation analysis, this increasing trend of annual average carbon
 375 stock exhibits a robust agreement with the dramatic increase in atmospheric CO₂ concentration
 376 ($R^2=0.9677$, $p<0.001$), suggesting that the carbon stock is strongly affected by CO₂ fertilization.

377 Meanwhile, the positive correlation between the carbon stock and CO₂ generally extends across LVBC
 378 ($R^2=0.9669$) and WVBC ($R^2=0.9622$). After the value of the global terrestrial carbon stock and trends
 379 were partitioned among the vegetation functional classes, we see that LVBC increases 116.18 ± 2.34 Pg
 380 C (or $\sim 15.60\%$), which explains 97.42% of total carbon stock increasing trend and dominates the positive
 381 global carbon stock trend; WVBC also increases 3.08 ± 0.14 Pg C (or $\sim 18.03\%$) over the past century.

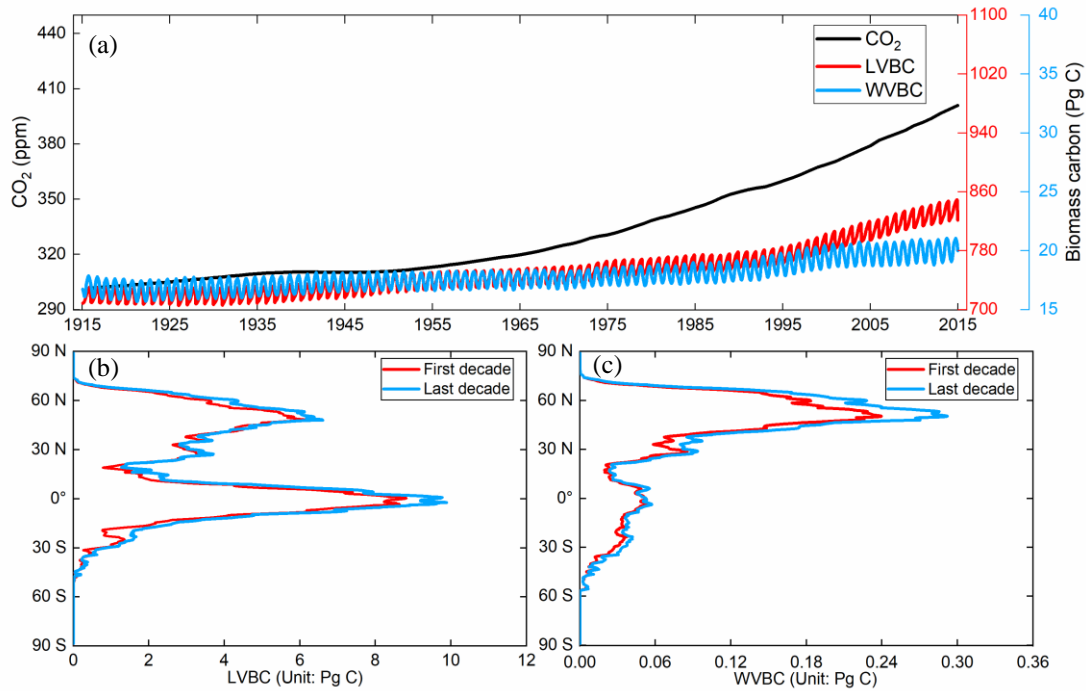


Figure 6. Global potential biomass carbon stocks of vegetation during the past 100 years. (a) The evolution of global potential biomass stocks (LVBC+WVBC), along with changes in biomass stocks that can be attributed to the variability and trend of LVBC and WVBC through the twentieth century. The red line represents the monthly value of LVBC, the blue line represents the monthly value of WVBC, and the black line represents the annual value of CO₂ concentration. (b, c) Zonal averaged sums of the annual LVBC and WVBC for latitudinal bands during the first decade (1916–1925, red line) and the last decade (2006–2015, blue line) shows the increased carbon stock capacity.

382 The global distributions of the decadal-average change in LVBC and WVBC are shown in Figures 6b
 383 and 6c, respectively. The significant historical changes in climate and CO₂ enhance the carbon stock of
 384 the terrestrial ecosystem, and their positive influences are broadly distributed across a latitudinal north–
 385 south gradient. The latitudinal bands of increasing annual LVBC are mainly distributed in the tropical
 386 and boreal latitudes, which is consistent with Figure 7b. The decadal and inter-annual variabilities of
 387 LVBC are dominated by the tropical and semi-arid/boreal zones where large portions of the zones are

388 highly productive (Ahlstrom et al., 2015; Poulter et al., 2014). Tropical LVBC dominates the long-term
389 trend of global LVBC in the last hundred years. Compared with LVBC, the increase of tropical WVBC
390 is light. There is a single peak in the spatial variation of annual WVBC (Figure 6c and Figure 7c). WVBC
391 exhibits robust growth at most latitudes, and increases mainly in boreal latitudes.

392 **3.3 Spatial variability in estimated LVBC and WVBC trends**

393 In Figures 7(a) and 7(b), total carbon stock and LVBC exhibited a significantly increasing trend in eastern
394 South America, southern Africa, and northern Asia, while they declined in central North America,
395 northwest South America, and central Africa. WVBC showed a more widely increasing tendency in
396 North America, southeastern South America, and Europe, while had a decreasing trend in part zones of
397 Asian. We find that the total carbon stock as well as the light- and water-gathering vegetation biomass
398 carbon stocks over the period of 1916–2015 exhibited a remarkable spatial heterogeneity. Figure 7a
399 shows that an increase in vegetation carbon stocks occurred over zones and global aggregate levels during
400 the entire study period. About 57.39% of the terrestrial grid cells exhibited an increase with a noticeable
401 trend ($p < 0.05$) in biomass carbon stock; 53.82% of global grid cells possessed increases that were
402 statistically significant at the $p = 0.01$ level. To determine the contributions of each fraction (LVBC,
403 WVBC) to the total change in the potential vegetation carbon stock, we partitioned and present the
404 historical spatial and temporal patterns for each fraction separately (Figure 7b, 7c). LVBC contributes
405 97.33% to the incremental change of total carbon stock (116.18 ± 2.34 Pg C), with about 51.32% of the
406 grid cells possessing a noticeable positive trend ($p = 0.01$). Generally, spatial patterns of LVBC and the
407 total carbon stock are consistent (Figure 7a, 7b), which further supports the argument that LVBC
408 dominates the trend in carbon stocks in most zones. Although the proportion of the total change in carbon
409 stocks is small (2.58% of total carbon stock increase), about 61.00% of the land surface shows an increase
410 in WVBC; of these terrestrial grid cells, 55.81% was characterized by a significant $p = 0.01$ increase.

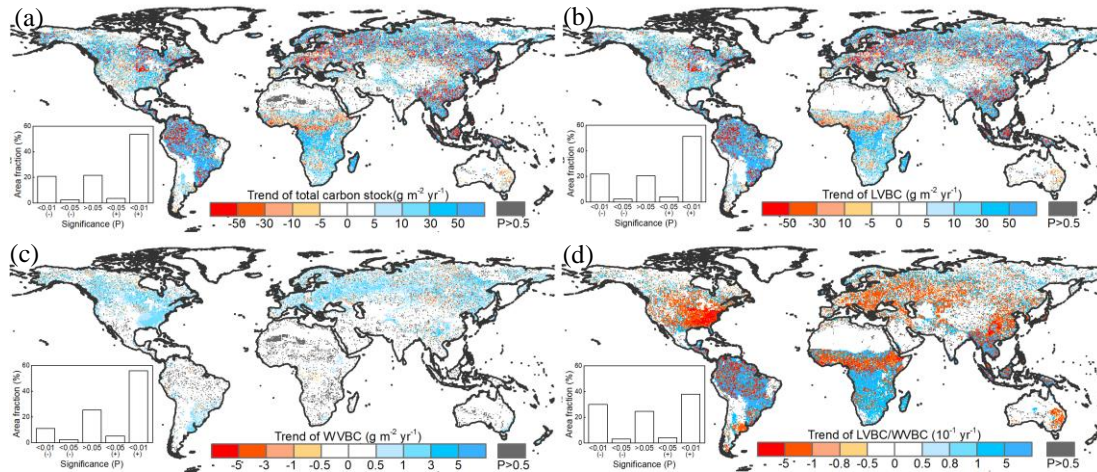


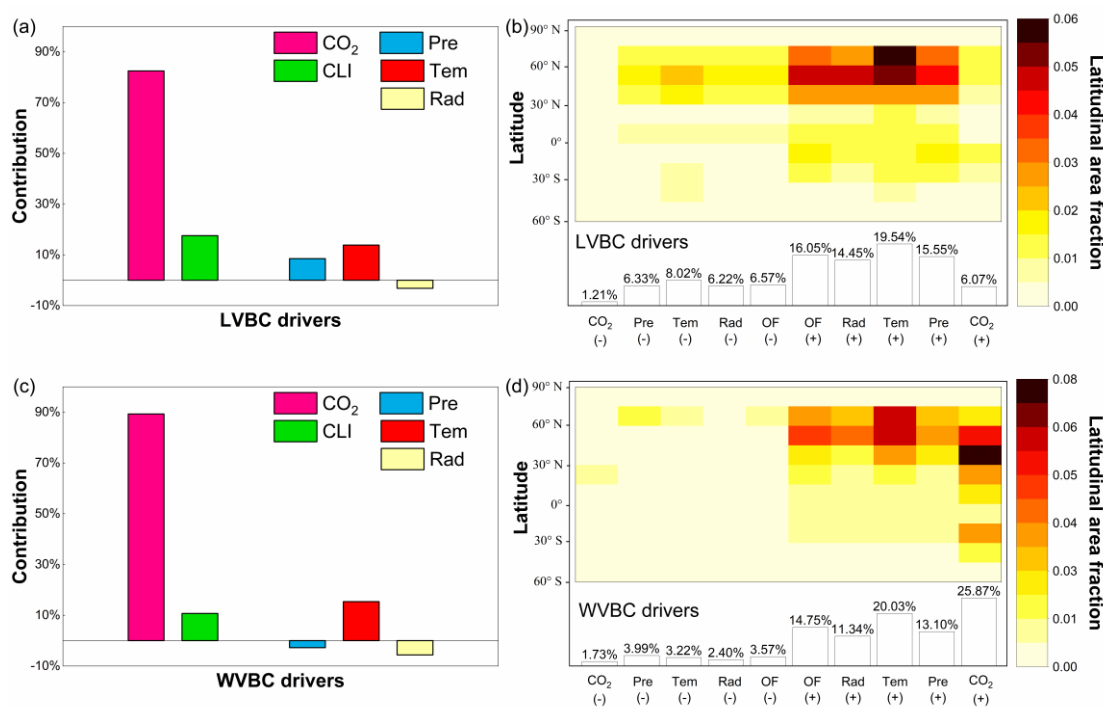
Figure 7. Spatial patterns in the trends of potential vegetation carbon stocks and their fractions from 1916 to 2015. Difference induced by changes in climate and CO₂ in terrestrial biomass carbon stock (a), LVBC (b), and WVBC (c) during the historic period 1916–2015. The blue bar indicates the significantly increasing trends and the red bar indicates the significantly decreasing trends in carbon stocks. (d) Trend in the LVBC/WVBC ratio from 1916 to 2015. The blue bar indicates significantly increasing trends in the ratio, and vice versa. The grey bar indicates the trend is statistically insignificant ($P > 0.05$). The sub-graphs show the significant test results. A ‘+’ symbol indicates a positive trend, and vice versa.

411 Under the influences of a changing climate and CO₂ concentrations, there is a slight increase in the ratio
 412 of global LVBC/WVBC; the rate of increase is 0.0171 yr⁻¹ in the last hundred years, which is significant
 413 at the 0.01 level (Figure 7d). About 42.08% of the terrestrial grid cells exhibits an increase with a
 414 noticeable trend ($p < 0.05$) in the ratio of LVBC and WVBC; 37.95% of global grid cells possessed
 415 increases that are statistically significant at the $p = 0.01$ level. Meanwhile, 33.32% of the land surface
 416 shows a significant decrease in LVBC/WVBC; of these terrestrial grid cells, 30.06% is characterized by
 417 a significant $p = 0.01$ decrease. Zones-Gird cells with noticeable increases in the ratio of LVBC to WVBC
 418 are mainly located in southern Africa, central South America, and northern Eurasia. Negative trends in
 419 LVBC/WVBC ratios are found in northern America, southern Europe, and tropical Africa.

420 3.4 Responses of LVBC and WVBC to environmental drivers

421 The responses of LVBC and WVBC to changes in climate and CO₂ are both positive at the global level
 422 (Figure 8a, 8c), although zonally, they exhibit both negative and positive responses (Figure 8b, 8d).
 423 Based on the results of factorial simulations and Mann-Kendall+Sen tests, CO₂ fertilization explains the

424 largest proportion of the change in the carbon stock; about 82.45% change in LVBC was positive (Figure
 425 8a), whereas 89.28% of the change in WVBC was positive (Figure 8c). In factorial simulation S2, the
 426 long-term trend of LVBC was $15.521 \text{ g C m}^{-2} \text{ yr}^{-1}$ and that of WVBC was $0.435 \text{ g C m}^{-2} \text{ yr}^{-1}$ at the
 427 period from 1916 to 2015 (Figure A2a and Figure A3a). The separately simulated LVBC and WVBC
 428 increased by 80.98 Pg C and 2.66 Pg C with increasing atmospheric CO₂ concentrations (from 301.73
 429 ppm in 1916 to 400.83 ppm in 2015). The other climatic drivers (precipitation, temperature, radiation,
 430 humidity, and wind speed) remained at baseline values. While the increase or decrease in the carbon
 431 stock may be attributed to more than one driving factor, within any specified grid cell, the one with the
 432 highest positive or negative contribution is the dominated-dominant driver that consistently resulted in
 433 the highest increase or decrease in the carbon stock for that grid cell. The spatial pattern illustrates that
 434 CO₂ dominates the variability in LVBC in 7.28% of the zones-grid cells, including 1.21% of the zones
 435 grid cells that exhibited a negative change and 6.07% that exhibited a positive change (Figure 8b). CO₂
 436 dominates the variability in WVBC in 27.60% of the zones-grid cells, including 1.73% of the zones-grid
 437 cells that exhibited a negative change and 25.87% of zones-grid cells with a positive change (Figure 8d).
 438 Under the effect of CO₂ fertilization, grid cells with increased trend in WVBC mainly distribute in boreal
 439 latitudes (Figure 6c). These trends are consistent with and previous studies (Tharammal et al., 2019; Zhu
 440 et al., 2016; Keenan et al., 2017) in which positive trends occurred, especially for WVBC.



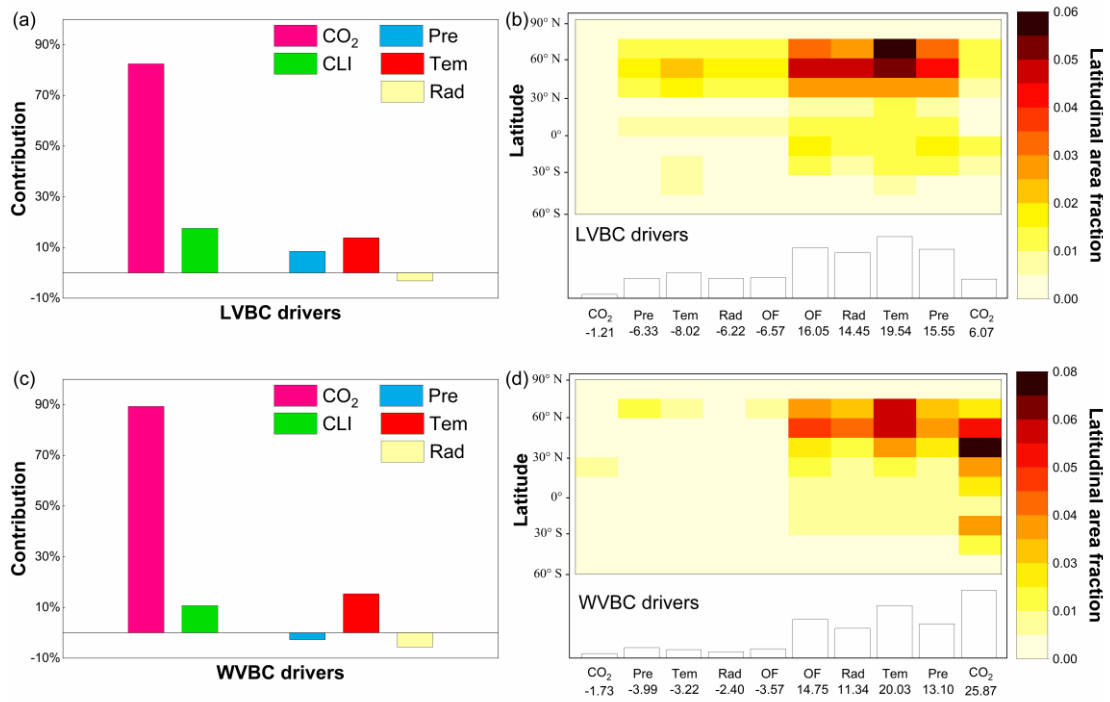
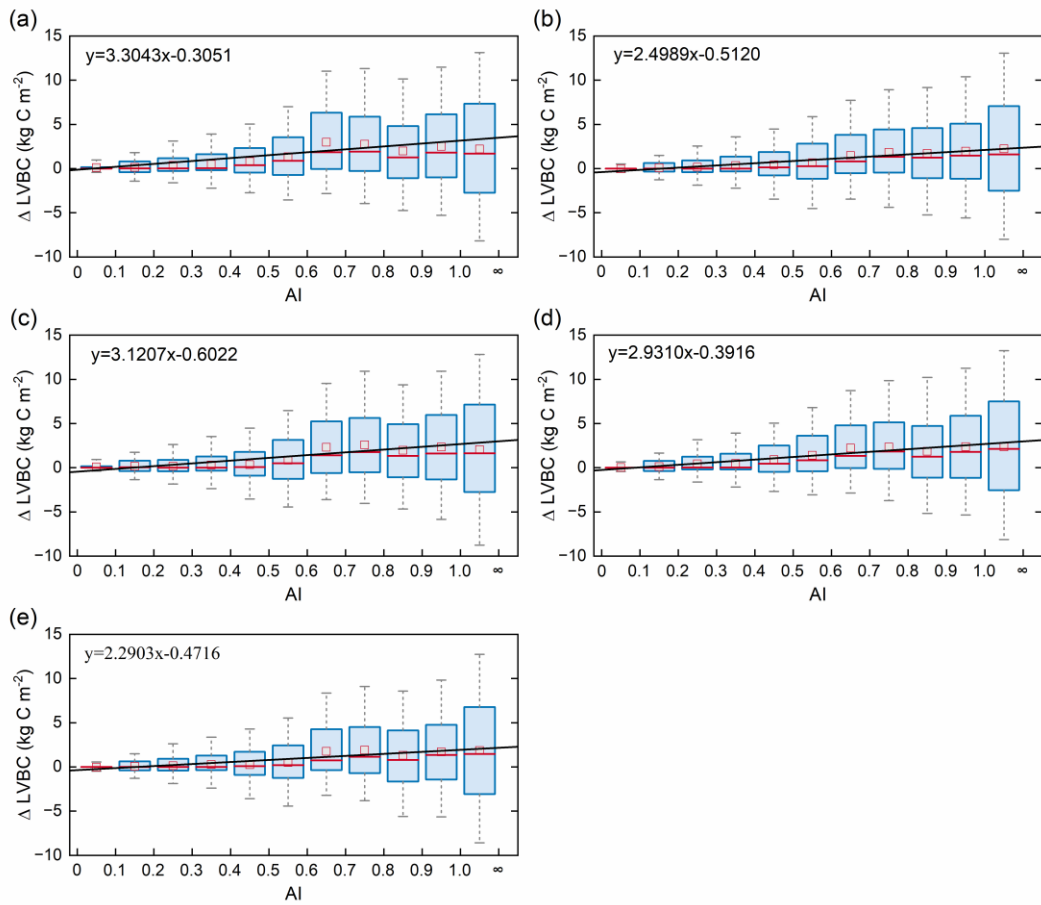


Figure 8. The proportion of changes in the vegetation biomass carbon stocks attributed to driving factors. Ratios of the driving factors of CO₂ fertilization effects (CO₂), climate change effects (CLI), precipitation (Pre), temperature (Tem), radiation (Rad) for LVBC (a) and WVBC (c) under the five scenarios using are calculated by the Mann-Kendall and Sen's slope estimator statistical tests. Attribution of LVBC (b) and WVBC (d) dynamics to driving factors calculated as averages along 15° latitude bands. At the local scales, the driving factors include CO₂, Pre, Tem, Rad, and other climate factors (OF). The fraction of global area-grid cells (%) that is predominantly influenced by the driving factors is showed at the bottom of the bar. The '-' symbol before fraction indicates a negative effect of the driving factor on carbon stock, and vice versa.

441 Climate change induced by the greenhouse effect explains part of the increase in carbon stocks, but unlike
 442 CO₂ fertilization, climate has dramatic negative effects on some vegetated zones. Figure 8a illustrates
 443 that temperature is the largest climatic contributor to the change in LVBC (13.83%, 2.572 g m⁻² yr⁻¹),
 444 followed by precipitation (8.51%, 1.572 g m⁻² yr⁻¹) and radiation (-3.19%, -0.649 g m⁻² yr⁻¹). The spatial
 445 distribution shows that temperature predominantly influences the change in LVBC (Figure 8b),
 446 influencing over 27.56% of the global vegetated zones-grid cells, followed by precipitation (21.88%) and
 447 radiation (20.67%). Figure 8c shows there are negative effects and contributions of precipitation on the
 448 change in WVBC at the global level (-2.76%, -0.013 g m⁻² yr⁻¹). Temperature is the largest climatic

449 contributor to the change in WVBC (15.36%, $0.075 \text{ g m}^{-2} \text{ yr}^{-1}$), followed by radiation (-5.63%, -0.027 g
450 $\text{m}^{-2} \text{ yr}^{-1}$). Modelled WVBC trends based on the factorial simulations have similar spatiotemporal patterns
451 to LVBC (Figures A2 and A3), and the spatial patterns of light- and water-gathering carbon stocks show
452 a significantly increasing trend in the most of boreal zones. In the Southern Hemisphere, the trends of
453 WVBC are extensively statistically insignificant in all factorial simulations, and only a small proportion
454 of grid cells show a significantly increasing trend. There is a significantly increasing trend in LVBC in
455 south-central Africa and northern South America. The effects of temperature on WVBC are stronger than
456 LVBC, because temperature has a stronger effect on the metabolism process of root growth, dominating
457 the turnover rate and the costs of maintenance respiration in root growth process (Gill and Jackson, 2000).
458 It should be noted that trends in the global carbon stock can be largely attributed to the influences of CO_2 ,
459 precipitation, temperature, and radiation (Figure 8). Nonetheless, at the zonal scale, the contributions of
460 other factors should be considered, such as humidity and wind speed. The effects of these other factors
461 dominate trends in LVBC in over 16.05% of the zones-grid cells that increased and 6.57% of the zones
462 grid cells that decreased. In the case of changes in WVBC, other factors were dominant drivers in over
463 14.75% of the zones-grid cells that increased and 3.57% of zones-grid cells that decreased. Under the
464 effect of climate, the variability of LVBC and WVBC is positive in most zonesgrid cells, promoting the
465 noticeable increase of carbon stocks in boreal latitudes.



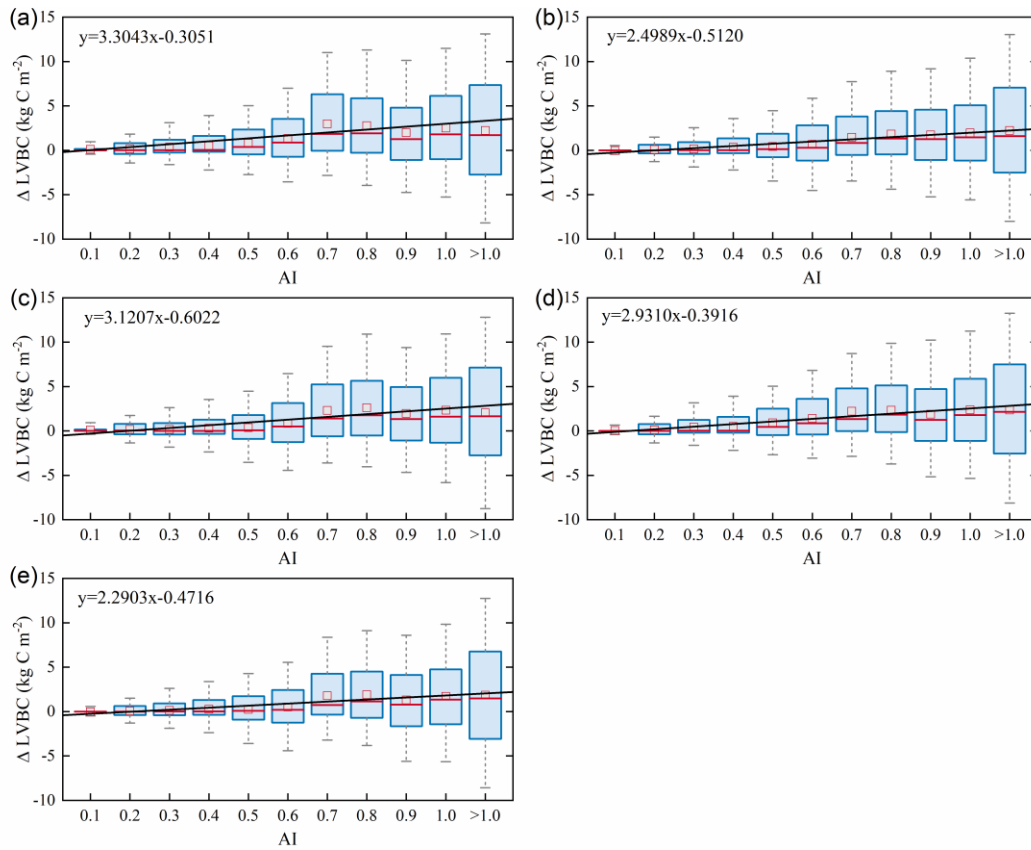


Figure 9. Relationships ~~in~~ of the incremental change between AI and LVBC ~~over the hydrological grid cells (Figure 1)~~. Magnitude of change in LVBC in the historical scenario S1 (a), CO₂ in scenario S2 (b), CO₂ + precipitation in scenario S3 (c), CO₂ + temperature in scenario S4 (d), and CO₂ + radiation in scenario S5 (e). ~~Range~~ The range of the box is 25%-75% of values; the range of the whiskers is 10%-90% of values; the small red square is average value; the red line is the median line; and the black line is the fitted curve. Positive value of the Y axis represents the magnitude of increased LVBC from 1916 to 2015 under water-limitations conditions, and vice versa. AI of grid cells is calculated by multiyear average precipitation and multiyear average potential evapotranspiration in the period of 1916-2015. Categories of hydrological zones include: hyper-arid (AI ≤ 0.05), arid (0.05 < AI ≤ 0.2), semi-arid (0.2 < AI ≤ 0.5), sub-humid (0.5 < AI ≤ 0.65), and humid (AI > 0.65).~~;~~

467 Terrestrial water availability emerged as a key regulator of terrestrial carbon storage, by affecting the
 468 response mechanism of the vegetation carbon stock to changes in driving factors. As shown in Figures 9
 469 and 10, with the accumulated change of LVBC and WVBC in the period of 1916 to 2015 across the
 470 aridity index (i.e., an increase in available water), the magnitude and range in responses of LVBC density

471 and WVBC density gradually increase. Based on the results of the historical simulation (Figure 9), we
472 find a positive relationship between LVBC and aridity index. In extreme water stress, the increase of
473 LVBC tends to zero and plants stop increasing their carbon storage. There is no obvious difference in
474 the slopes of fitting curves between factorial simulations, which shows the robustness in the response of
475 LVBC to the change of water stress. The pattern of the enhanced magnitude and range of variation in the
476 WVBC density is unimodal with water stress gradient in all factorial simulations. With the increasing of
477 AI, the magnitude of change in WVBC increases at first and then decreases finally. The mitigation of
478 water stress promotes WVBC increase, while excess surface water limits the response of WVBC to
479 changes in climate and CO₂. These results reveal that the carbon stock increases stimulated by changes
480 in climate and CO₂ are constrained by water available. With increased warming, water limitations are
481 expected to increasingly limit the carbon stock increase, specially at arid regions. To further reveal the
482 controls of water limitation on the responses of inner carbon storages to each driver, we analyse the long-
483 term variability of potential vegetation carbon stocks by means of factorial simulations for each
484 hydrological region (Figure 1). Figure A7b shows that the ~~maximum change magnitude~~fluctuation range
485 (the difference between maximum value and minimum value in each factorial simulation) of LVBC
486 density across all factorial simulation is 1.202 kg C m⁻² in the hyper-arid regions for the 1916-2015
487 period. As shown in Figure A7f, the ~~maximum change magnitude~~fluctuation range of LVBC density in
488 humid regions is 6.068 kg C m⁻² during the same period. —In Figure A8b, the maximum change
489 magnitude of WVBC density across all factorial simulation is 0.011 kg C m⁻² in the hyper-arid regions
490 during the time of 1916-2015. In Figure A8f, the maximum change magnitude of WVBC density is 0.046
491 kg C m⁻² in humid regions during the same period. Compared with plants ~~lived~~ in aridity regions, plants
492 in humid regions show more dramatic responses to the stimulation from drivers' change. With a lessening
493 of water stress (from hyper-arid to humid region), the response magnitudes of the carbon stock to the
494 changes of climate and CO₂ gradually become more noticeable. The robust pattern in the zonal average
495 density of the carbon stock shows that terrestrial water limitations strongly regulate the enhanced
496 magnitude of the carbon stock.

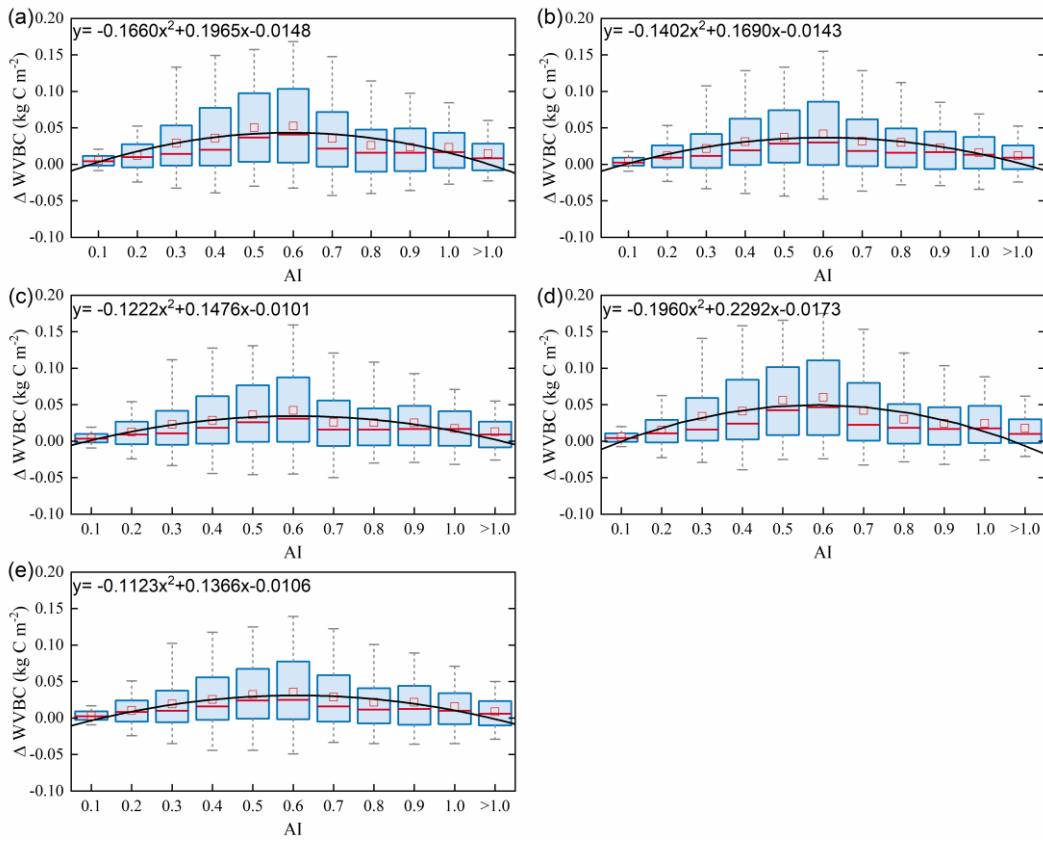
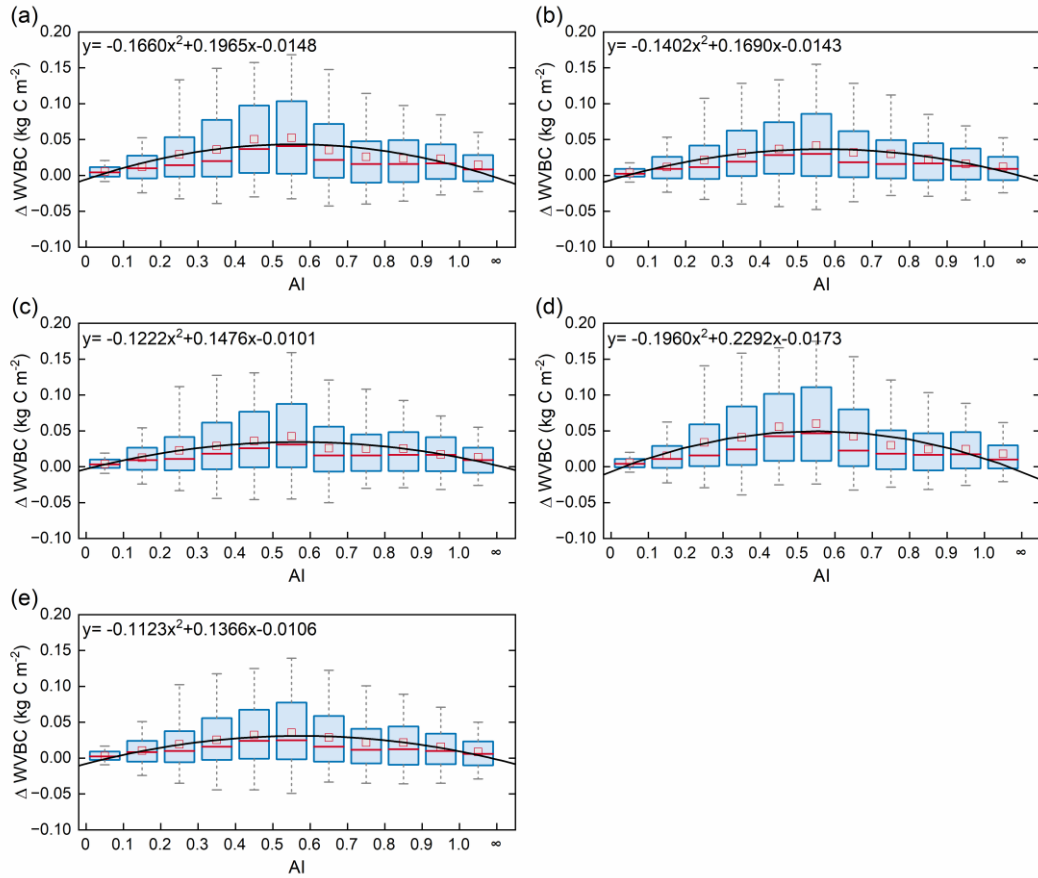


Figure 10. Relationships ~~in~~ of the incremental change in AI and WVBC ~~over the hydrological grid cells (Figure 1).~~ Magnitude of change in WVBC in the historical scenario S1 (a), CO₂ in scenario S2 (b), CO₂ + precipitation in scenario S3 (c), CO₂ + temperature in scenario S4 (d), and CO₂ + radiation in scenario S5 (e). ~~The R~~range of the box is 25%-75% of values; ~~the~~ range of the whiskers is 10%-90% of values; the small red square is average value; the red line is the median line, and the black line is the fitted curve. Positive value of the Y axis represents the magnitude of increased WVBC from 1916 to 2015 under water-limitations conditions, and vice versa. AI of grid cells is calculated by multiyear average precipitation and multiyear average potential evapotranspiration in the period of 1916-2015. Categories of hydrological zones include: hyper-arid ($AI \leq 0.05$), arid ($0.05 < AI \leq 0.2$), semi-arid ($0.2 < AI \leq 0.5$), sub-humid ($0.5 < AI \leq 0.65$), and humid ($AI > 0.65$).

497 Water limitations not only directly reduced the magnitude of the response in the two fractions' carbon
 498 stock (LVBC and WVBC) to changes in climate and CO₂, but also indirectly confined the response
 499 direction of each fractions' carbon stock by transforming vegetation structure and function. Figure 11
 500 illustrates temporal variations in the carbon stock ratio within and between hydrological regions. From
 501 hyper-arid ~~zones~~ regions to humid ~~zones~~ regions, the fluctuation range ~~(the difference between maximum~~
 502 ~~value and minimum value in each factorial simulation)~~ of LVBC/WVBC ratio significantly changes. The
 503 fluctuation magnitudes of LVBC/WVBC in humid and hyper-arid ~~zones~~ regions are greater than that in
 504 other hydrological ~~zones~~ regions. Compared with plants in hyper-arid ~~zones~~ regions, plants in humid
 505 ~~zones~~ regions exhibit more significant responses to changes in climate and CO₂. Meanwhile, the long-
 506 term effects of driver changes have a remarkable influence on this carbon allocation pattern at global
 507 level (Figure 7d). Under the synergistic effect of drivers and water stress, the trends of light- and water-
 508 gathering vegetation carbon stock are upward in the past hundred years (Figure 6). However, there is a
 509 difference in the increasing rate between LVBC and WVBC, resulting in a dramatic and complicated
 510 fluctuation in global LVBC/WVBC ratio (Figure 11a). ~~Whereas LVBC decreases and WVBC increases~~
 511 ~~in hyper-arid and arid regions (Fig. A7 and A8), causing a downward trend in LVBC:WVBC ratio,~~
 512 ~~semiarid regions see an increase in LVBC. The density of LVBC decreases and that of WVBC increases~~
 513 ~~in hyper-arid and arid zones for all factorial simulations (Figures A7 and A8).~~ So, the ratio of LVBC and
 514 WVBC shows a downward trend in these ~~zones~~ regions. LVBC in semi-arid regions shows upward
 515 tendency in the past years (Figure A7d) because of the aridity mitigation. There is an upward trend in

516 WVBC in semi-arid regions (Figure A8d). Plants in semi-arid regions still utilize a tolerance strategy
 517 and allocates more non-structural carbon to water-gathering vegetation organ to resist water stress,
 518 resulting in the decline of LVBC/WVBC ratio. In humid zones/regions, light- and water-gathering
 519 biomass carbon stocks both increased in all factorial simulations (Figures A7 and A8). The proportion
 520 of LVBC increases more than that of WVBC for capturing more resources like CO₂ and radiation energy,
 521 leading to an increase in the LVBC/WVBC ratio. The value of LVBC/WVBC in S3 is higher than that
 522 in S4 and S5, which represents that precipitation makes more contributions to the change of
 523 LVBC/WVBC ratio among meteorological factors.

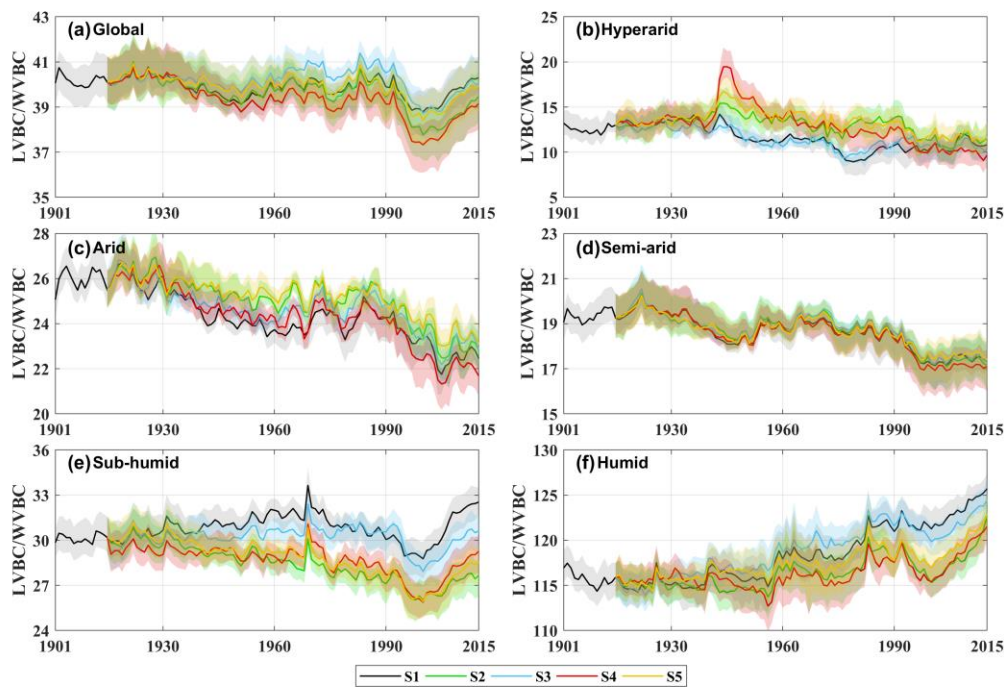


Figure 11. Temporal fluctuations in carbon stock dynamics in vegetation biomass in different factorial simulations. Black indicates historical factorial simulation from 1901-2015, green indicates the CO₂-driven factorial simulation, blue indicates the precipitation-driven factorial simulation, red indicates the temperature-driving factorial simulation and yellow indicates radiation driven factorial simulation. Uncertainty bounds are provided as shaded areas reflect the intra-annual fluctuation (± 1 s.d.) (a) Modelled trend of LVBC/WVBC ratio in Global area. (b-f) Modelled trend of the LVBC/WVBC ratio in different hydrological regions (Figure 1).

524 4 Discussions and conclusion

525 To understand the response of carbon storage potential and its inner biomass carbon stocks to
526 environmental change, we conducted a series of factorial simulations using SEIB-DGVM V3.02. More
527 importantly, we investigated the extent of the responses of carbon stocks to water limitations.

528

529 Over the past 100 years, there has been an ongoing increase in the carbon storage capacity of the
530 terrestrial ecosystem from 735 Pg C in 1916 to 855 Pg C in 2015 (Figure 6), which has slowed the rate
531 at which atmospheric CO₂ has increased and may have mitigated global warming. These findings are
532 consistent with the conclusions of research conducted at the local scale. For example, based on carbon
533 flux data, Erb et al. (2008) suggested that the vegetation carbon stock in Austria increased from 1043 Mt
534 C to 1249 Mt C (aboveground carbon stocks growth was 1.059 Mt C yr⁻¹ and belowground carbon stocks
535 growth was 0.2 Mt C yr⁻¹) since industrialization. Le Noë et al. (2020) showed that increases in the
536 carbon stocks and carbon density were the predominant drivers in the forest terrestrial carbon
537 sequestration capacity in France from 1850 to 2015. Tong et al. (2020) also found a substantial increase
538 of aboveground carbon stocks in southern China (0.11 Pg C yr⁻¹) during the period 2002–2017. However,
539 these studies focused on zonal trends in total vegetation carbon stocks and did not investigate the extent
540 of the response in vegetation carbon stocks partitioned between light- and water-gathering biomass. Our
541 results show that the increase in carbon stock in light-gathering vegetation organs was much larger than
542 that in water-gathering vegetation organs, and light-gathering biomass carbon stock dominates the
543 historical trend of the terrestrial carbon stock. During the past decades, the global land surface has been
544 greening because of the flux and storage of more carbon into plant trunks and foliage (Zhu et al., 2016).
545 LVBC increases 116.18 ± 2.34 Pg C from 1916 to 2015, accounting for 97.42% of the total carbon stock
546 increase (119.26 ± 2.44 Pg C). The long-term trends and spatial pattern of vegetation carbon stock ~~are~~
547 predominated the variability characteristic of LVBC. The latitudinal bands of increasing annual change
548 in LVBC are mainly distributed in tropical latitudes, a conclusion consistent with prior knowledge that
549 tropical zones dominate carbon uptake and storage (Erb et al., 2018; Schimel et al., 2015). ~~Under the~~
550 ~~influences of environmental stressors, WVBC increases significantly in boreal latitudes.~~ Biomass carbon
551 allocation between light- and water-gathering vegetation organs reflect the changes in individual growth,
552 community structure and ecosystem function, which are important attributes in the investigation of

553 carbon stocks and carbon cycling within the terrestrial biosphere (Hovenden et al., 2014; Fang et al.,
554 2010; Ma et al., 2021). During the past hundred years, the ratio of LVBC/WVBC showed a slight upward
555 trend since LVBC increased relatively more ~~—dramatically—~~ than WVBC. The rate of increase is 0.0171
556 yr⁻¹, which is significant at the 0.01 level. To better absorb CO₂ and sunlight required for photosynthesis,
557 vegetated regions are gradually covered by vegetation with higher plant height and wider leaf area,
558 thereby adjusting their characteristic ecosystem functions (Erb et al., 2008).

559

560 Based on our factorial simulations (Figure 8), the influences of CO₂ fertilization induce the most
561 significant variation of the vegetation carbon stock. In addition, the responses of carbon stocks to the
562 changes of climatic factors are obvious, particularly at the zonal-grid cell scale. Previous studies have
563 pointed out that the variation of the terrestrial carbon stock caused by releasing or sequestering carbon is
564 sensitive to anomalous changes in water availability and light use efficiency (Madani et al., 2020;

565 Humphrey et al., 2018). ~~At the grid-cell scale, shown in Figure 8b and 8d, radiation and precipitation
566 dominate the long-term trend of carbon stocks over one-third of global grid cells. At the global scale,
567 radiation and precipitation explain approximately 10% of long-term trend in LVBC and WVBC (Figure
568 8a and 8c). LVBC and WVBC variations driven by precipitation and radiation are ultimately offset by
569 spatially compensatory effects, which dampens the response of the carbon stock to these factors at global
570 scale (Jung et al., 2017). This spatially compensatory effect of climate changes is consistent with previous
571 analyses (Zhu et al., 2016) that climate changes explain 8% of the increasing carbon storage of global
572 foliage, while climate changes dominate the greening trend over 28.4% of the global land. Results reveal
573 that trends in temperature drove historical long-term trends in the potential carbon stocks, with faster
574 increases and considerable variation occurring by zone. The accumulated influence of climate warming
575 induces dramatic changes in the carbon stock at a global scale. Thus, we suggest that temperature
576 dominates the long-term trends in the carbon stock among climatic drivers, while a compensatory effect
577 exists in the global change in the carbon stock induced by precipitation and radiation. At the grid cell
578 scale, as shown in Figures 8b and 8d, temperature, radiation, precipitation, and other climate factors
579 (humidity and wind speed) dominate the long-term trend of carbon stocks over two thirds of global grid
580 cells. At the global scale, climate factors explain 17.55% and 10.72% of long-term trend in LVBC and
581 WVBC, respectively (Figures 8a and 8c). LVBC and WVBC variations driven by climate factors are~~

582 ultimately offset by spatially compensatory effects, which dampens the response of the carbon stock to
583 these factors at the global scale (Jung et al., 2017). Thus, contributions of precipitation and radiation to
584 the variability of LVBC and WVBC are relatively low at the global scale, and the effects of humidity
585 and wind speed on global carbon stock are minor. This spatially compensatory effect of climate changes
586 is consistent with a previous analysis (Zhu et al. 2016) which found that climate changes explain only 8%
587 of the increasing trend in foliage carbon storage at the global level but that they dominate the trend over
588 28.4% of global land area. Results show that trends in temperature drive historical long-term trends in
589 the potential carbon stocks, with faster increases and considerable variation occurring by grid cell. Thus,
590 our results reveal that temperature dominates the long-term trends of carbon stock among climatic drivers,
591 while a relatively strong compensatory effect exists in the global change in the carbon stock induced by
592 precipitation, radiation, humidity, and wind speed.

593

594 By partitioning the trends of LVBC and WVBC into five hydrological regions (Figure 1), we found that
595 the long-term change in carbon stocks is tightly coupled to terrestrial water availability. These results
596 indicate that vegetation in humid regions is responsible for most of the trend in global LVBC, while
597 plants in semi-arid regions play a dominate global role in controlling the long-term trend in WVBC
598 (Figures 9 and 10). As water stress decreases, the magnitude and range in variation of LVBC gradually
599 increase (Figure 9), which suggests that limited water availability constrains the response magnitude of
600 the changes in LVBC to changes in CO₂ and climate. The response pattern of WVBC growth to the
601 increasing water availability is different from that of LVBC. Drought mitigation promotes the growth of
602 WVBC. In sub-humid and humid regions, plants face low water limitations and intensified light-
603 competition and have to invest as much non-structural carbon as possible into leaf and trunk. This
604 allocation scheme leads to the decreased investment of Δ WVBC in wet regions. The result is consistent
605 with previous finding that plants reduce investment to roots in dense forests where aboveground
606 competition for light is high (Ma et al. 2021). Moreover, we found that indirect effects of water limitation
607 regulate increasing rate of each carbon pool. Although vegetation carbon stocks dramatically increase
608 under the effects of climate and CO₂ changes, the increasing rate of LVBC faster than WVBC in humid
609 regions. Vegetation stores more biomass in aboveground plant organs (trunk and foliage) to gather light.
610 Dryland plants decrease the LVBC/WVBC ratios and store more biomass below ground to enhance the

611 capture of water resources. Based on these results, we demonstrate that water limitations controlled the
612 variable response of terrestrial vegetation carbon stocks.

613

614 Our findings are consistent with other reports about the impact of increasing water limitations on
615 terrestrial ecosystem. Based on observation from satellite remote sensing ~~observations~~, Madani et al.
616 (2020) found that the constraining impact of water limitation determines whether global ecosystem
617 productivity responds positively or negatively to the changes in climate factors. Madani et al. (2020)
618 ~~found that changes in water constraints significantly affect the response patterns of ecosystem~~
619 ~~productivity and net carbon exchange.~~ Humphrey et al. (2021) found that increasing water stress limits
620 the response magnitude of carbon uptake rates through a down-regulation of stomatal conductance and
621 suggested that land carbon uptake is driven by temperature and vapour pressure deficit effects that are
622 controlled by terrestrial water availability. Ma et al. (2021) found that plants increase investment into
623 building roots in arid region because the extent of water limitation there is exacerbated by global warming.
624 Terrestrial hydrological conditions significantly affect the carbon cycle ~~process~~ of terrestrial ecosystems,
625 including carbon uptake, allocation, and stock. Terrestrial ecosystems utilize sensitive strategies to
626 allocate and store biomass to adjust to local hydrological conditions. A significant conclusion is that
627 water constraints not only confine the responses of vegetation carbon stocks to drivers ~~of variability~~, but
628 also constrain the proportion of biomass carbon stocks in gather- and water-gathering fractions.

629

630 Distinguishing the response of carbon stock fractions estimated by SEIB-DGVM improves the
631 understanding of the interactive impacts of terrestrial carbon and water dynamics. However, uncertainty
632 still exists because of the limitations in the processes of modelling vegetation metabolism with SEIB-
633 DGVM. Trunk biomass contains tree branches and structural roots (coarse roots and tap roots) (Sato et
634 al., 2007), so the R/S ratio of potential vegetation in factorial simulations is smaller than the R/S of actual
635 vegetation in observation stations. Root biomass only contains the fine root biomass, leading to an
636 apparent underestimate in belowground organ biomass of trees and grasses compare with previous
637 conclusion (Ma et al., 2021; Yang et al., 2009). Availability of nitrogen is a key limiting factor for
638 vegetation growth, especially when higher CO₂ fertilization effects exist (Tharammal et al., 2019). The
639 limitation could be alleviated by nitrogen deposition in most temperate and boreal ecosystems. The

640 SEIB-DGVM experiments were conducted with a focus on documenting CO₂ fertilization and climate
641 change interactions; these experiments did not consider the influences of nitrogen deposition, which ~~leads~~
642 ~~to a slight~~ should cause an underestimate of the contributions of CO₂ fertilization on biomass production.

643

644 In summary, we evaluated SEIB-DGVM V3.02 and used this model to offer new perspectives on the
645 response of vegetation carbon storage potential to changes in climate and CO₂. Our simulation results
646 show that changes in CO₂, rather than climate, dominate the light- and water-gathering partitioning of
647 the carbon storage potential. More importantly, we suggest that the impact of CO₂ fertilization and
648 temperature effects on vegetation carbon-sequestration potential depends on water availability and its
649 impacts on plant stress. With increased global warming, water limitations are expected to increasingly
650 confine global carbon sequestration and storage. Our findings highlight the need to account for terrestrial
651 water limitation effects when estimating the response of the terrestrial carbon storage capacity to global
652 climate change, and the need for stronger interactions between those involved in vegetation model
653 development and those in between the hydrological and ecological research communities.

655 **Table A1. MCD12C1 legend and class descriptions**

Name	Value	Description
Evergreen Needleleaf Forests	1	Dominated by evergreen conifer trees (canopy >2m). Tree cover >60%.
Evergreen Broadleaf Forests	2	Dominated by evergreen broadleaf and palmate trees (canopy >2m). Tree cover >60%.
Deciduous Needleleaf Forests	3	Dominated by deciduous needleleaf (larch) trees (canopy >2m). Tree cover >60%.
Deciduous Broadleaf Forests	4	Dominated by deciduous broadleaf trees (canopy >2m). Tree cover >60%.
Mixed Forests	5	Dominated by neither deciduous nor evergreen (40-60% of each) tree type (canopy >2m). Tree cover >60%.
Closed Shrublands	6	Dominated by woody perennials (1-2m height) >60% cover.
Open Shrublands	7	Dominated by woody perennials (1-2m height) 10-60% cover.
Woody Savannas	8	Tree cover 30-60% (canopy >2m).
Savannas	9	Tree cover 10-30% (canopy >2m).
Grasslands	10	Dominated by herbaceous annuals (<2m).
Permanent Wetlands	11	Permanently inundated lands with 30-60% water cover and >10% vegetated cover.
Croplands	12	At least 60% of area is cultivated cropland.
Urban and Built-up Lands	13	At least 30% impervious surface area including building materials, asphalt, and vehicles.
Cropland/Natural Vegetation Mosaics	14	Mosaics of small-scale cultivation 40-60% with natural tree, shrub, or herbaceous vegetation.
Permanent Snow and Ice	15	At least 60% of area is covered by snow and ice for at least 10 months of the year.
Barren	16	At least 60% of area is non-vegetated barren (sand, rock, soil) areas with less than 10% vegetation.
Water Bodies	17	At least 60% of area is covered by permanent water bodies.
Unclassified	255	Has not received a map label because of missing inputs

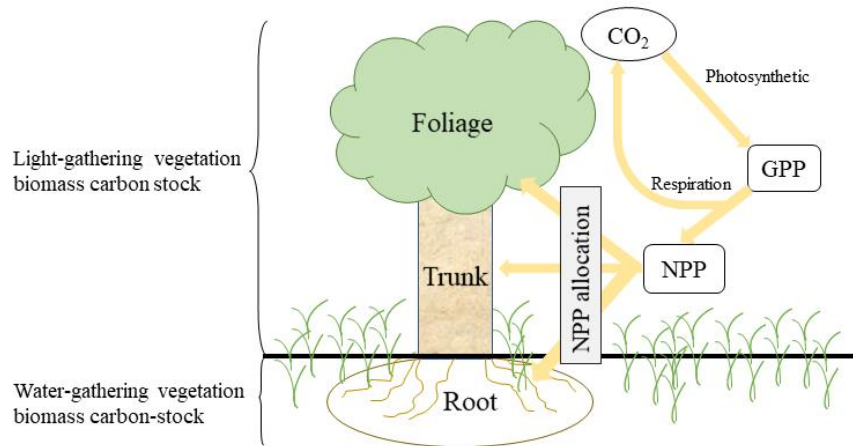


Figure A1. Schematic of ecosystem carbon cycle. Yellow arrow indicates carbon flux. Atmospheric CO₂ transitions into gross primary production (GPP) by photosynthesis. GPP is partitioned into respiration and net primary production (NPP). NPP is partitioned into three biomass carbon pools (foliage, trunk, and root).

657

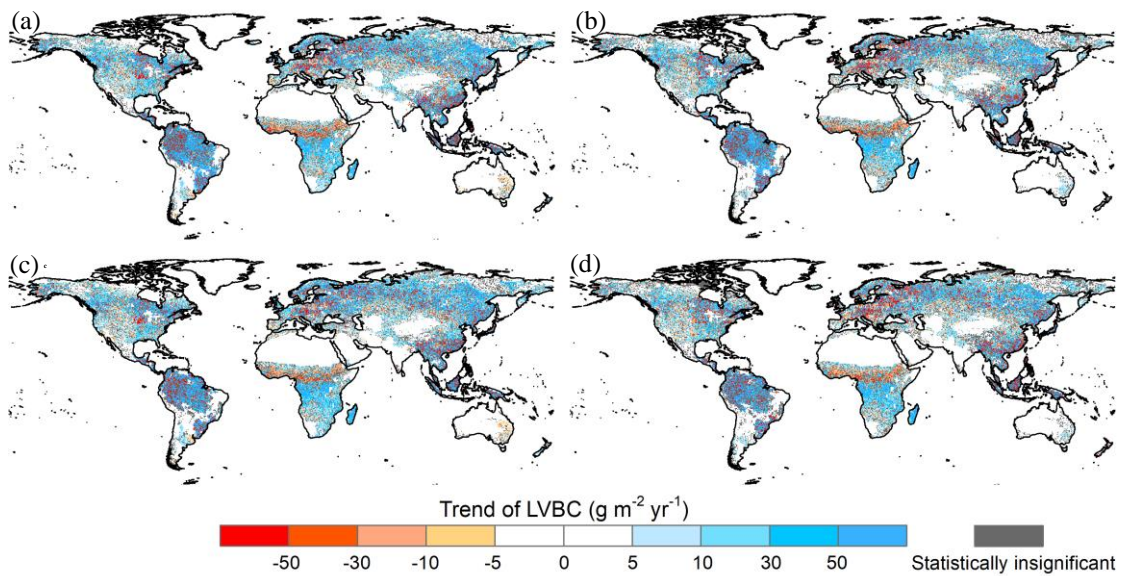


Figure A2. Potential LVBC trend maps during the period of 1916 to 2015 under different factorial simulations. (a) CO₂ driving factorial simulation (S2); (b) CO₂+precipitation driving factorial simulation (S3); (c) CO₂+temperature driving factorial simulation (S4); and (d) CO₂+radiation driving factorial simulation (S5). Positive values indicate increasing trends in the ratio, and vice versa. All results from Mann-Kendall and Sen's slope statistical tests correspond to the 95% confidence interval.

658

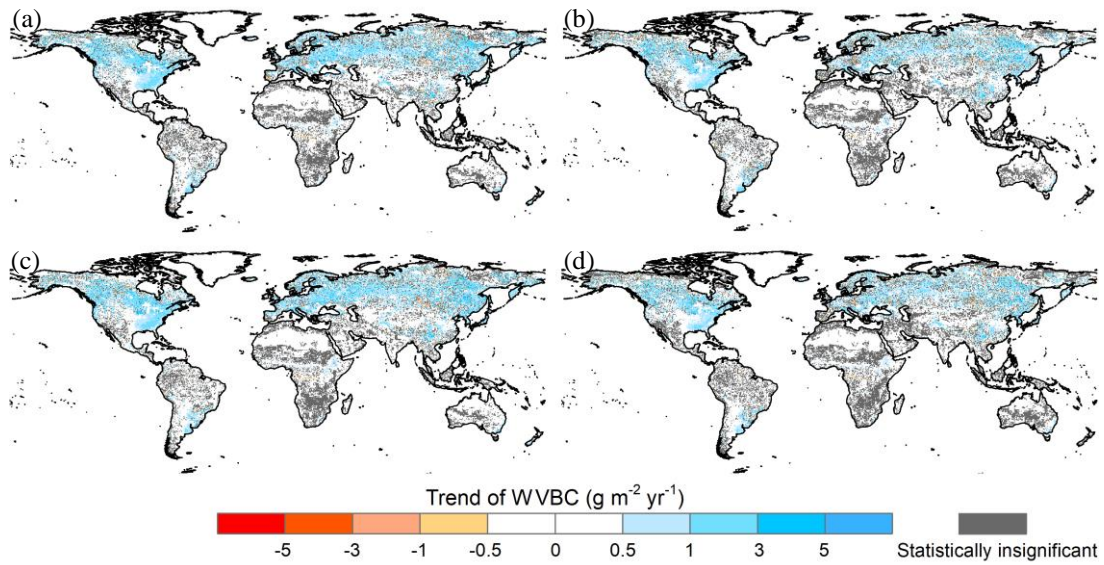


Figure A3. Potential WVBC variation trend maps during the period of 1916 to 2015 under different factorial simulations. (a) CO_2 driving factorial simulation (S2); (b) CO_2 +precipitation driving factorial simulation (S3); (c) CO_2 +temperature driving factorial simulation (S4); and (d) CO_2 +radiation driving factorial simulation (S5). Positive values indicate increasing trends in the ratio, and vice versa. All results from Mann-Kendall and Sen's slope statistical tests correspond to the 95% confidence interval.

659

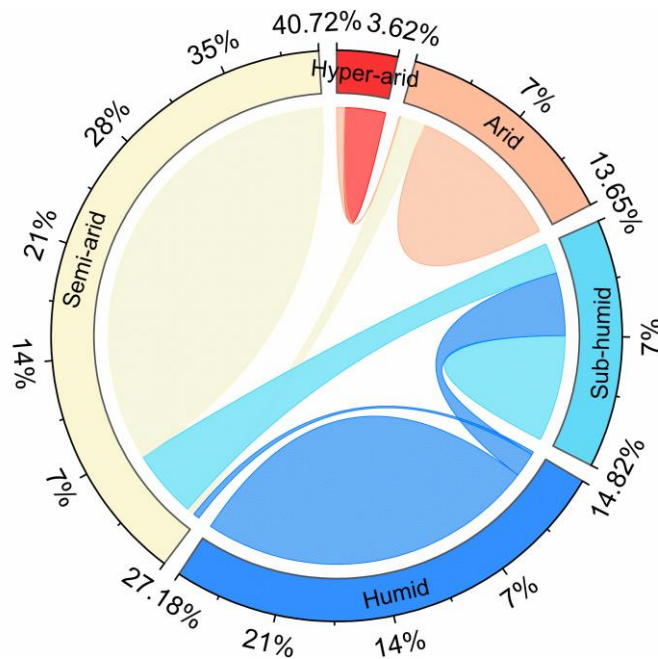


Figure A4. The shift of hydrological regions defined by the multiyear average AI index from the period of 1916-1945 to the period of 1986-2015. The outermost number represent the percentage of hydrological regions in 1916-1945.

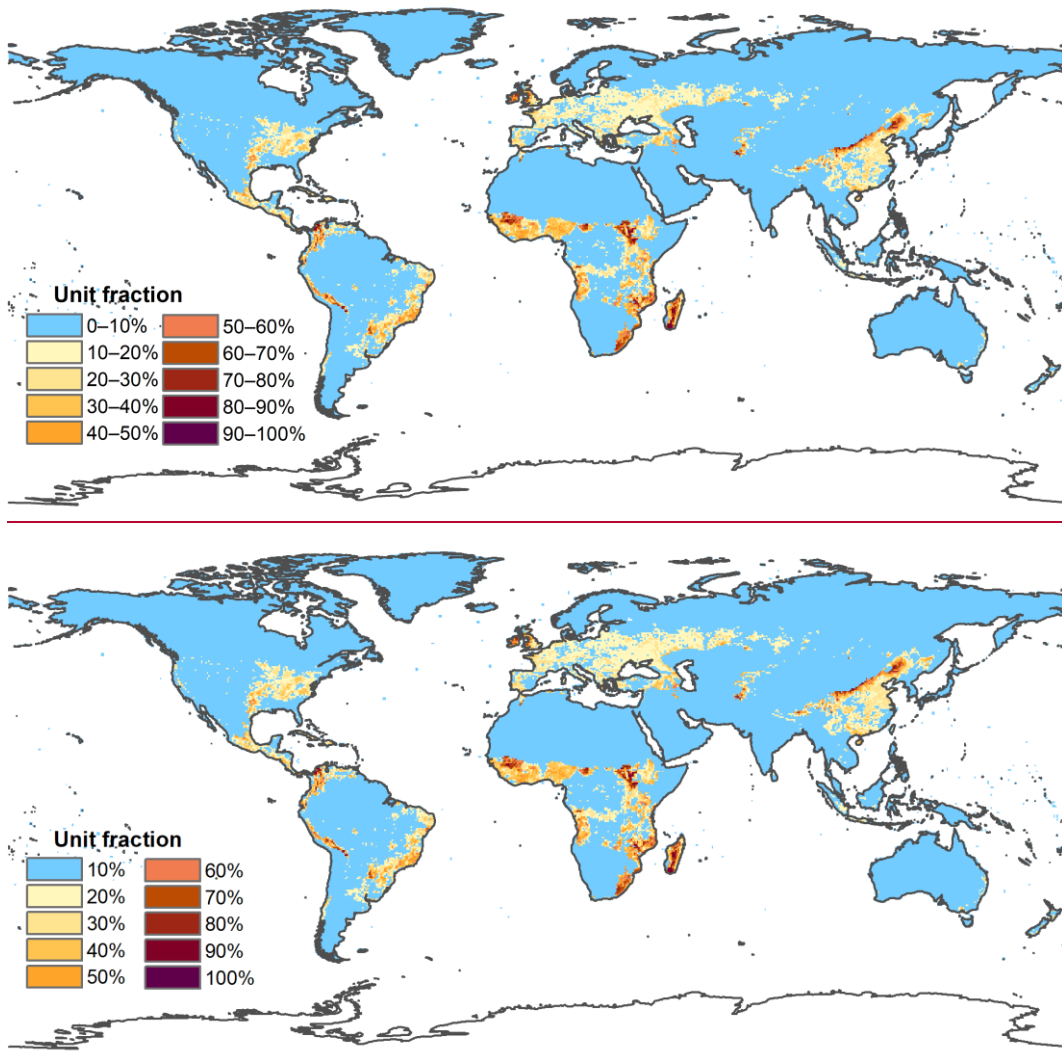


Figure A5. Spatial distribution of multi-year average fraction of managed pasture from 2001-2015 at 0.5 x 0.5 arc-degree resolution.

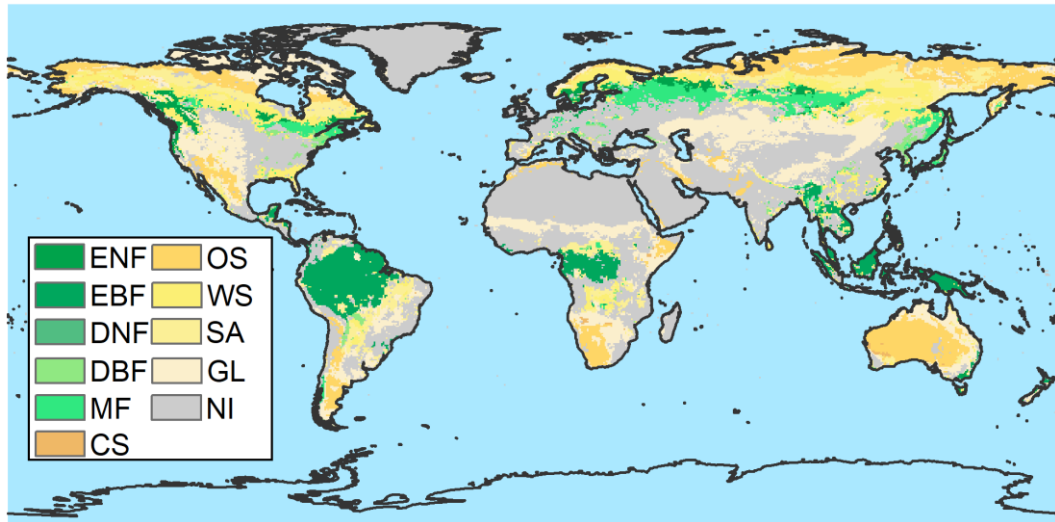


Figure A6. Map of grid cells whose largest vegetation component without anthropogenic disturbance from MCD12C1 and LUH2. ENF: Evergreen needleleaf forest, EBF: Evergreen broadleaf forest, DNF: Deciduous needleleaf forest, DBF: Deciduous broadleaf forest, MF: Mixed forest, CS: Closed shrublands, OS: Open shrublands, WS: Woody savannas, SA: Savannas, GL: Grasslands, NI: Not included, which means the zone is not covered by vegetation without anthropogenic disturbance.

662

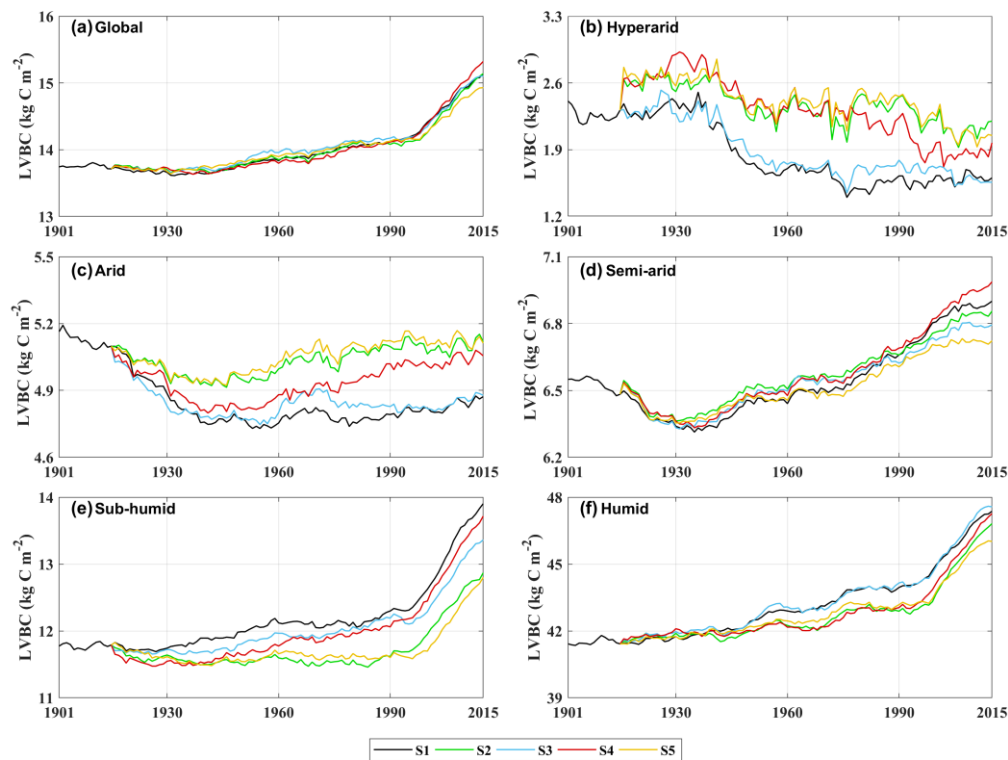


Figure A7. Trends in average density of potential LVBC. (a) Modelled trend of annual averaged LVBC globally. Modelled trends in annual averaged LVBC in hyper-arid zone-region (b), arid zone-region (c), semi-arid zone-region (d), sub-humid zone-region (e), and humid zone-region (f).

663

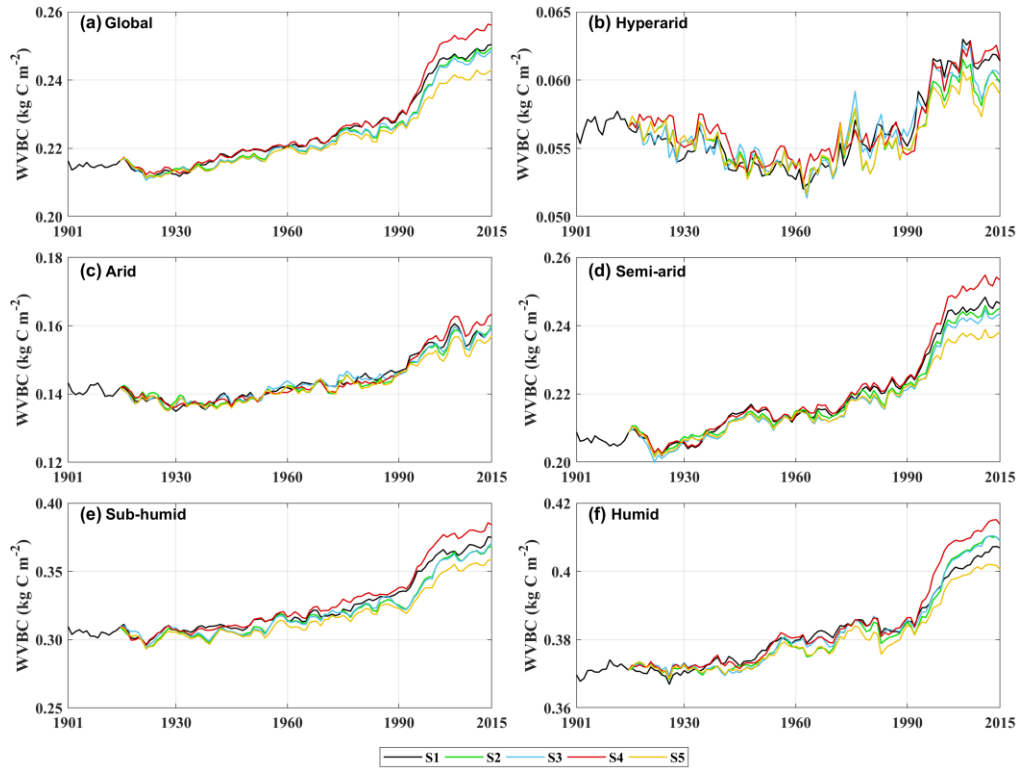


Figure A8. Trends in average density of potential WVBC. (a) Modelled trend of annual averaged WVBC globally. Modelled trends in annual averaged WVBC in hyper-arid zone-region (b), arid zone-region (c), semi-arid zone-region (d), sub-humid zone-region (e), and humid zone-region (f).

664 **Code and data availability statement**

665 The code of SEIB-DGVM version 3.02 can be download from <http://seib-dgvm.com/>. Climatic Research
 666 Unit data can be downloaded from <https://crudata.uea.ac.uk/cru/data/hrg/>. The soil physical parameters
 667 can be downloaded from www.iges.org/gswp. The reconstructed CO₂ concentration dataset and SEIB
 668 code can be downloaded from <http://seib-dgvm.com/>. In model validation, Ecosystem Model-Data
 669 Intercomparison (multiyear average NPP product) data were collected from
 670 https://daac.ornl.gov/NPP/guides/NPP_EMDI.html. Remote sensing product MOD17A3 data were
 671 obtained from <https://lpdaac.usgs.gov/products/mod17a3hgf006/>, MCD12C1 data were obtained from

672 <https://ladsweb.modaps.eosdis.nasa.gov/search/order>, and LUH2 data were obtained from
673 <https://luh.umd.edu/>.

674 **Authors contributions**

675 T.S. designed research. T.S., and S.H. performed research and developed the methodology. T.S. analyzed
676 data and produced the outputs. T.S., S.H., C.J., and X.C. wrote the first manuscript draft. W.W. and W.G.
677 supervised the study. All the authors discussed the methodology and commented on various versions of
678 the manuscript.

679 **Competing interests**

680 The authors declare that they have no conflict of interest.

681 **Acknowledgments**

682 This work was jointly supported by the National Natural Science Foundation of China (Grant Nos.
683 51979071, 51779073, 91547205), the National Key Research and Development Program of China
684 (2021YFC3201100), the Distinguished Young Fund Project of Natural Science Foundation of Jiangsu
685 Province (BK20180021), and the National “Ten Thousand Program” Youth Talent. We thank Zefeng
686 Chen for technical support. We gratefully thank the following data providers and model developers for
687 their continuous efforts and for sharing their data: the University of East Anglia, the National Centers for
688 Environmental Prediction (NCEP), the National Oceanic and Atmospheric Administration (NOAA),
689 University of Maryland, and the Center for Ocean-Land-Atmosphere Studies (COLA). Cordial thanks
690 are extended to the editor, Dr. Hans Verbeeck, and two anonymous referees for the valuable comments
691 which greatly improve the quality of the paper.

692 **References**

- 693 Ahlstrom, A., Raupach, M. R., Schurgers, G., Smith, B., Arneth, A., Jung, M., Reichstein, M., Canadell,
 694 J. G., Friedlingstein, P., Jain, A. K., Kato, E., Poulter, B., Sitch, S., Stocker, B. D., Viovy, N., Wang,
 695 Y. P., Wiltshire, A., Zaehle, S., and Zeng, N.: The dominant role of semi-arid ecosystems in the
 696 trend and variability of the land CO₂ sink, *Science*, 348, 895-899, 10.1126/science.aaa1668, 2015.
- 697 Ajtay, G. L., Ketner, P., and Duvigneaud, P.: Terrestrial primary production and phytomass In: *The*
 698 *Global Cycle.*, Glob. Carbon Cycle, SCOPE, 129-181 pp.1979.
- 699 Bartholome, E. and Belward, A. S.: GLC2000: a new approach to global land cover mapping from Earth
 700 observation data, *Int J Remote Sens*, 26, 1959-1977, 10.1080/01431160412331291297, 2005.
- 701 Bayer, A. D., Pugh, T. A. M., Krause, A., and Arneth, A.: Historical and future quantification of
 702 terrestrial carbon sequestration from a Greenhouse-Gas-Value perspective, *Global Environmental*
 703 *Change*, 32, 153-164, 10.1016/j.gloenvcha.2015.03.004, 2015.
- 704 Bazilevich, N. I., Rodin, L. Y., and Rozov, N. N.: Geographical Aspects of Biological Productivity,
 705 *Soviet Geograpy Review and Translation*, 5, 293-317 pp.1971.
- 706 Bloom, A. A., Exbrayat, J. F., van der Velde, I. R., Feng, L., and Williams, M.: The decadal state of the
 707 terrestrial carbon cycle: Global retrievals of terrestrial carbon allocation, pools, and residence times,
 708 *Proceedings of the National Academy of Sciences of the United States of America*, 113, 1285-1290,
 709 10.1073/pnas.1515160113, 2016.
- 710 Chen, J., Ju, W., Ciais, P., Viovy, N., Liu, R. G., Liu, Y., and Lu, X. H.: Vegetation structural change
 711 since 1981 significantly enhanced the terrestrial carbon sink, *Nat Commun*, 10, 4259,
 712 10.1038/S41467-019-12257-8, 2019.
- 713 Chen, L.-P., Zhao, N.-X., Zhang, L.-H., and Gao, Y.-B.: Responses of two dominant plant species to
 714 drought stress and defoliation in the Inner Mongolia Steppe of China, *Plant Ecology*, 214, 221-229,
 715 10.1007/s11258-012-0161-y, 2013.
- 716 Cheng, L., Zhang, L., Wang, Y. P., Canadell, J. G., Chiew, F. H. S., Beringer, J., Li, L. H., Miralles, D.
 717 G., Piao, S. L., and Zhang, Y. Q.: Recent increases in terrestrial carbon uptake at little cost to the
 718 water cycle, *Nat Commun*, 8, 10.1038/s41467-017-00114-5, 2017.
- 719 Erb, K.-H., Gingrich, S., Krausmann, F., and Haberl, H.: Industrialization, Fossil Fuels, and the
 720 Transformation of Land Use, *Journal of Industrial Ecology*, 12, 686-703, 10.1111/j.1530-
 721 9290.2008.00076.x, 2008.
- 722 Erb, K.-H., Gaube, V., Krausmann, F., Plutzar, C., Bondeau, A., and Haberl, H.: A comprehensive global
 723 5min resolution land-use data set for the year 2000 consistent with national census data, *Journal of*
 724 *Land Use Science*, 2, 191-224, 10.1080/17474230701622981, 2007.
- 725 Erb, K.-H., Fetzel, T., Plutzar, C., Kastner, T., Lauk, C., Mayer, A., Niedertscheider, M., Körner, C., and
 726 Haberl, H.: Biomass turnover time in terrestrial ecosystems halved by land use, *Nat Geosci*, 9, 674-
 727 678, 10.1038/ngeo2782, 2016.
- 728 Erb, K.-H., Kastner, T., Plutzar, C., Bais, A. L. S., Carvalhais, N., Fetzel, T., Gingrich, S., Haberl, H.,
 729 Lauk, C., Niedertscheider, M., Pongratz, J., Thurner, M., and Luyssaert, S.: Unexpectedly large
 730 impact of forest management and grazing on global vegetation biomass, *Nature*, 553, 73-76,
 731 10.1038/nature25138, 2018.
- 732 Fan, L., Wigneron, J. P., Ciais, P., Chave, J., Brandt, M., Fensholt, R., Saatchi, S. S., Bastos, A., Al-
 733 Yaari, A., Hufkens, K., Qin, Y. W., Xiao, X. M., Chen, C., Myneni, R. B., Fernandez-Moran, R.,
 734 Mialon, A., Rodriguez-Fernandez, N. J., Kerr, Y., Tian, F., and Penuelas, J.: Satellite-observed

735 pantropical carbon dynamics, *Nat Plants*, 5, 944-951, 10.1038/s41477-019-0478-9, 2019.

736 Fang, J., Yang, Y., Ma, W., Mohammat, A., and Shen, H.: Ecosystem carbon stocks and their changes
737 in China's grasslands, *Science China. Life sciences*, 53, 757-765, 10.1007/s11427-010-4029-x, 2010.

738 Friedlingstein, P., Joel, G., Field, C. B., and Fung, I. Y.: Toward an allocation scheme for global
739 terrestrial carbon models, *Global Change Biol*, 5, 755-770, DOI 10.1046/j.1365-2486.1999.00269.x,
740 1999.

741 Gentine, P., Green, J. K., Guérin, M., Humphrey, V., Seneviratne, S. I., Zhang, Y., and Zhou, S.:
742 Coupling between the terrestrial carbon and water cycles—a review, *Environ Res Lett*, 14, 083003,
743 10.1088/1748-9326/ab22d6, 2019.

744 Gill, R. and Jackson, R.: Global patterns of root turnover for terrestrial ecosystems, *New Phytol*, 147,
745 13-31, 10.1046/j.1469-8137.2000.00681.x, 2000.

746 Gocic, M. and Trajkovic, S.: Analysis of changes in meteorological variables using Mann-Kendall and
747 Sen's slope estimator statistical tests in Serbia, *Global and Planetary Change*, 100, 172-182,
748 10.1016/j.gloplacha.2012.10.014, 2013.

749 Gulbeyaz, O., Bond-Lamberty, B., Akyurek, Z., and West, T. O.: A new approach to evaluate the MODIS
750 annual NPP product (MOD17A3) using forest field data from Turkey, *Int J Remote Sens*, 39, 2560-
751 2578, 10.1080/01431161.2018.1430913, 2018.

752 Haberl, H., Erb, K. H., and Krausmann, F.: Human Appropriation of Net Primary Production: Patterns,
753 Trends, and Planetary Boundaries, *Annu Rev Env Resour*, 39, 363-391, 10.1146/annurev-environ-
754 121912-094620, 2014.

755 Harper, A. B., Wiltshire, A. J., Cox, P. M., Friedlingstein, P., Jones, C. D., Mercado, L. M., Sitch, S.,
756 Williams, K., and Duran-Rojas, C.: Vegetation distribution and terrestrial carbon cycle in a carbon
757 cycle configuration of JULES4.6 with new plant functional types, *Geosci Model Dev*, 11, 2857-
758 2873, 10.5194/gmd-11-2857-2018, 2018.

759 Harris, I., Osborn, T. J., Jones, P., and Lister, D.: Version 4 of the CRU TS monthly high-resolution
760 gridded multivariate climate dataset, *Scientific Data*, 7, 109, 10.1038/s41597-020-0453-3, 2020.

761 Hovenden, M. J., Newton, P. C., and Wills, K. E.: Seasonal not annual rainfall determines grassland
762 biomass response to carbon dioxide, *Nature*, 511, 583-586, 10.1038/nature13281, 2014.

763 Humphrey, V., Zscheischler, J., Ciais, P., Gudmundsson, L., Sitch, S., and Seneviratne, S. I.: Sensitivity
764 of atmospheric CO₂ growth rate to observed changes in terrestrial water storage, *Nature*, 560, 628-
765 631, 10.1038/s41586-018-0424-4, 2018.

766 Humphrey, V., Berg, A., Ciais, P., Gentine, P., Jung, M., Reichstein, M., Seneviratne, S. I., and
767 Frankenberg, C.: Soil moisture–atmosphere feedback dominates land carbon uptake variability,
768 *Nature*, 592, 65-69, 10.1038/s41586-021-03325-5, 2021.

769 Hurtt, G. C., Chini, L. P., Frolking, S., Betts, R. A., Feddema, J., Fischer, G., Fisk, J. P., Hibbard, K.,
770 Houghton, R. A., Janetos, A., Jones, C. D., Kindermann, G., Kinoshita, T., Goldewijk, K. K., Riahi,
771 K., Shevliakova, E., Smith, S., Stehfest, E., Thomson, A., Thornton, P., van Vuuren, D. P., and
772 Wang, Y. P.: Harmonization of land-use scenarios for the period 1500-2100: 600 years of global
773 gridded annual land-use transitions, wood harvest, and resulting secondary lands, *Climate Change*,
774 109, 117-161, 10.1007/s10584-011-0153-2, 2011.

775 Hurtt, G. C., Chini, L., Sahajpal, R., Frolking, S., Bodirsky, B. L., Calvin, K., Doelman, J. C., Fisk, J.,
776 Fujimori, S., Goldewijk, K. K., Hasegawa, T., Havlik, P., Heinemann, A., Humpenöder, F.,
777 Jungclauss, J., Jed Kaplan, Kennedy, J., Kristzin, T., Lawrence, D., Lawrence, P., Ma, L., Mertz, O.,
778 Pongratz, J., Popp, A., Poulter, B., Riahi, K., Shevliakova, E., Stehfest, E., Thornton, P., Tubiello,

779 F. N., van Vuuren, D. P., Zhang, X.: Harmonization of Global Land-Use Change and Management
780 for the Period 850-2100 (LUH2) for CMIP6, *Geoscientific Model Development*, 13, 5425-5464,
781 10.5194/gmd-13-5425-2020, 2021.

782 IPCC: Impacts, Adaptation and Vulnerability. Contribution of Working Group II to the Fourth
783 Assessment Report of the Intergovernmental Panel on Climate Change, 2007.

784 Jung, M., Reichstein, M., Schwalm, C. R., Huntingford, C., Sitch, S., Ahlstrom, A., Arneeth, A., Camps-
785 Valls, G., Ciais, P., Friedlingstein, P., Gans, F., Ichii, K., Jain, A. K., Kato, E., Papale, D., Poulter,
786 B., Raduly, B., Rodenbeck, C., Tramontana, G., Viovy, N., Wang, Y. P., Weber, U., Zaehle, S., and
787 Zeng, N.: Compensatory water effects link yearly global land CO₂ sink changes to temperature,
788 *Nature*, 541, 516-520, 10.1038/nature20780, 2017.

789 Kaplan, J. O., Krumhardt, K. M., Ellis, E. C., Ruddiman, W. F., Lemmen, C., and Goldewijk, K. K.:
790 Holocene carbon emissions as a result of anthropogenic land cover change, *Holocene*, 21, 775-791,
791 10.1177/0959683610386983, 2011.

792 Keenan, T. F., Prentice, I. C., Canadell, J. G., Williams, C. A., Wang, H., Raupach, M., and Collatz, G.
793 J.: Recent pause in the growth rate of atmospheric CO₂ due to enhanced terrestrial carbon uptake
794 *Nat Commun*, 7, 10.1038/Ncomms16137, 2017.

795 Kindermann, G. E., Mcallum, I., Fritz, S., and Obersteiner, M.: A global forest growing stock, biomass
796 and carbon map based on FAO statistics, *Silva Fenn*, 42, 387-396, 10.14214/Sf.244, 2008.

797 Le Noë, J., Matej, S., Magerl, A., Bhan, M., Erb, K. H., and Gingrich, S.: Modeling and empirical
798 validation of long-term carbon sequestration in forests (France, 1850-2015), *Glob Chang Biol*, 26,
799 2421-2434, 10.1111/gcb.15004, 2020.

800 Liu, J., Bowman, K. W., Schimel, D. S., Parazoo, N. C., Jiang, Z., Lee, M., Bloom, A. A., Wunch, D.,
801 Frankenberg, C., Sun, Y., O'Dell, C. W., Gurney, K. R., Menemenlis, D., Gierach, M., Crisp, D.,
802 and Eldering, A.: Contrasting carbon cycle responses of the tropical continents to the 2015-2016 El
803 Nino, *Science*, 358, eaam5690, 10.1126/science.aam5690, 2017.

804 Ma, H. Z., Mo, L. D., Crowther, T. W., Maynard, D. S., van den Hoogen, J., Stocker, B. D., Terrer, C.,
805 and Zohner, C. M.: The global distribution and environmental drivers of aboveground versus
806 belowground plant biomass, *Nat Ecol Evol*, 5, 1110+, 10.1038/s41559-021-01485-1, 2021.

807 Madani, N., Parazoo, N. C., Kimball, J. S., Ballantyne, A. P., Reichle, R. H., Maneta, M., Saatchi, S.,
808 Palmer, P. I., Liu, Z., and Tagesson, T.: Recent Amplified Global Gross Primary Productivity Due
809 to Temperature Increase Is Offset by Reduced Productivity Due to Water Constraints, *AGU*
810 *Advances*, 2, e2020AV000180, 10.1029/2020AV000180, 2020.

811 Magerl, A., Le Noë, J., Erb, K.-H., Bhan, M., and Gingrich, S.: A comprehensive data-based assessment
812 of forest ecosystem carbon stocks in the U.S. 1907–2012, *Environ Res Lett*, 14, 125015,
813 10.1088/1748-9326/ab5cb6, 2019.

814 McConnaughay, K. D. M. and Coleman, J. S.: Biomass allocation in plants: ontogeny or optimality? A
815 test along three resource gradients, *Ecology*, 80, 2581-2593, 10.1890/0012-
816 9658(1999)080[2581:BAIPOO]2.0.CO;2, 1999.

817 Monteith, J. L. and Unsworth, M. H.: *Principles of Environmental Physics*, 2nd ed., London 1990.

818 Olson, J., Watts, J., and Allison, L.: *Carbon in Live Vegetation of Major World Ecosystems*, Oak Ridge
819 National Laboratory 1983.

820 Pan, Y. D., Birdsey, R. A., Phillips, O. L., and Jackson, R. B.: The Structure, Distribution, and Biomass
821 of the World's Forests, *Annu Rev Ecol Evol S*, 44, 593-622, 10.1146/annurev-ecolsys-110512-
822 135914, 2013.

823 Pan, Y. D., Birdsey, R. A., Fang, J. Y., Houghton, R., Kauppi, P. E., Kurz, W. A., Phillips, O. L.,
824 Shvidenko, A., Lewis, S. L., Canadell, J. G., Ciais, P., Jackson, R. B., Pacala, S. W., McGuire, A.
825 D., Piao, S. L., Rautiainen, A., Sitch, S., and Hayes, D.: A Large and Persistent Carbon Sink in the
826 World's Forests, *Science*, 333, 988-993, 10.1126/science.1201609, 2011.

827 Piao, S. L., Friedlingstein, P., Ciais, P., Zhou, L. M., and Chen, A. P.: Effect of climate and CO₂ changes
828 on the greening of the Northern Hemisphere over the past two decades, *Geophys Res Lett*, 33,
829 L23402, 10.1029/2006GL028205, 2006.

830 Piao, S. L., Wang, X., Wang, K., Li, X., Bastos, A., Canadell, J. G., Ciais, P., Friedlingstein, P., and
831 Sitch, S.: Interannual variation of terrestrial carbon cycle: Issues and perspectives, *Glob Chang Biol*,
832 26, 300-318, 10.1111/gcb.14884, 2020.

833 Poorter, H.: Construction costs and payback time of biomass: a whole plant perspective, *A Whole-Plant
834 Perspective on Carbon-Nitrogen Interactions*, SPB Academic Publishing, The Hague 1994.

835 Poulter, B., Frank, D., Ciais, P., Myneni, R. B., Andela, N., Bi, J., Broquet, G., Canadell, J. G., Chevallier,
836 F., Liu, Y. Y., Running, S. W., Sitch, S., and van der Werf, G. R.: Contribution of semi-arid
837 ecosystems to interannual variability of the global carbon cycle, *Nature*, 509, 600-603,
838 10.1038/nature13376, 2014.

839 Prentice, I. C., Harrison, S. P., and Bartlein, P. J.: Global vegetation and terrestrial carbon cycle changes
840 after the last ice age, *New Phytol*, 189, 988-998, 10.1111/j.1469-8137.2010.03620.x, 2011.

841 Roy, J., Saugier, B., and Mooney, H. A.: Estimations of global terrestrial productivity: converging toward
842 a single number? In: *Terrestrial Global Productivity*, Academic Press, San Diego 2001.

843 Ruesch, A. and Gibbs, H. K.: New IPCC Tier-1 global biomass carbon map for the year 2000, 2008.

844 Ryan, M. G.: Effects of Climate Change on Plant Respiration, *Ecological Applications*, 1, 157-167,
845 10.2307/1941808, 1991.

846 Sato, H., Itoh, A., and Kohyama, T.: SEIB-DGVM: A new Dynamic Global Vegetation Model using a
847 spatially explicit individual-based approach, *Ecological Modelling*, 200, 279-307,
848 10.1016/j.ecolmodel.2006.09.006, 2007.

849 Sato, H., Kobayashi, H., Beer, C., and Fedorov, A.: Simulating interactions between topography,
850 permafrost, and vegetation in Siberian larch forest, *Environ Res Lett*, 15, 095006, 10.1088/1748-
851 9326/Ab9be4, 2020.

852 Saugier, B., Roy, J., and Mooney, H.: Estimations of Global Terrestrial Productivity, *Terrestrial Global
853 Productivity*, Academic Press, San Diego, Calif 2001.

854 Schimel, D., Stephens, B. B., and Fisher, J. B.: Effect of increasing CO₂ on the terrestrial carbon cycle,
855 *Proceedings of the National Academy of Sciences of the United States of America*, 112, 436-441,
856 10.1073/pnas.1407302112, 2015.

857 Seo, H. and Kim, Y.: Interactive impacts of fire and vegetation dynamics on global carbon and water
858 budget using Community Land Model version 4.5, *Geosci Model Dev*, 12, 457-472, 10.5194/gmd-
859 12-457-2019, 2019.

860 Shevliakova, E., Pacala, S. W., Malyshev, S., Hurtt, G. C., Milly, P. C. D., Caspersen, J. P., Sentman, L.
861 T., Fisk, J. P., Wirth, C., and Crevoisier, C.: Carbon cycling under 300 years of land use change:
862 Importance of the secondary vegetation sink, *Global Biogeochem Cy*, 23, 10.1029/2007gb003176,
863 2009.

864 Sun, F., Roderick, M. L., and Farquhar, G. D.: Changes in the variability of global land precipitation,
865 *Geophys Res Lett*, 39, L19402, 10.1029/2012gl053369, 2012.

866 Tei, S., Sugimoto, A., Liang, M. C., Yonenobu, H., Matsuura, Y., Osawa, A., Sato, H., Fujinuma, J., and

867 Maximov, T.: Radial Growth and Physiological Response of Coniferous Trees to Arctic
868 Amplification, *J Geophys Res-Bioge*, 122, 2786-2803, 10.1002/2016JG003745, 2017.

869 Terrer, C., Phillips, R. P., Hungate, B. A., Rosende, J., Pett-Ridge, J., Craig, M. E., van Groenigen, K. J.,
870 Keenan, T. F., Sulman, B. N., Stocker, B. D., Reich, P. B., Pellegrini, A. F. A., Pendall, E., Zhang,
871 H., Evans, R. D., Carrillo, Y., Fisher, J. B., Van Sundert, K., Vicca, S., and Jackson, R. B.: A trade-
872 off between plant and soil carbon storage under elevated CO₂, *Nature*, 591, 599-603,
873 10.1038/s41586-021-03306-8, 2021.

874 Tharammal, T., Bala, G., Devaraju, N., and Nemani, R.: A review of the major drivers of the terrestrial
875 carbon uptake: model-based assessments, consensus, and uncertainties, *Environ Res Lett*, 14,
876 093005, 10.1088/1748-9326/Ab3012, 2019.

877 Tong, X. W., Brandt, M., Yue, Y. M., Ciais, P., Jepsen, M. R., Penuelas, J., Wigner, J. P., Xiao, X.
878 M., Song, X. P., Horion, S., Rasmussen, K., Saatchi, S., Fan, L., Wang, K. L., Zhang, B., Chen, Z.
879 C., Wang, Y. H., Li, X. J., and Fensholt, R.: Forest management in southern China generates short
880 term extensive carbon sequestration, *Nat Commun*, 11, 10.1038/s41467-019-13798-8, 2020.

881 West, P. C., Gibbs, H. K., Monfreda, C., Wagner, J., Barford, C. C., Carpenter, S. R., and Foley, J. A.:
882 Trading carbon for food: Global comparison of carbon stocks vs. crop yields on agricultural land,
883 *Proceedings of the National Academy of Sciences of the United States of America*, 107, 19645-
884 19648, 10.1073/pnas.1011078107, 2010.

885 Wild, M., Gilgen, H., Roesch, A., Ohmura, A., Long, C. N., Dutton, E. G., Forgan, B., Kallis, A., Russak,
886 V., and Tsvetkov, A.: From dimming to brightening: Decadal changes in solar radiation at Earth's
887 surface, *Science*, 308, 847-850, 10.1126/science.1103215, 2005.

888 Yang, Y., Fang, J., Ma, W., Guo, D., and Mohammat, A.: Large-scale pattern of biomass partitioning
889 across China's grasslands, *Global Ecology and Biogeography*, 19, 268-277, 10.1111/j.1466-
890 8238.2009.00502.x, 2010.

891 Zhang, H., Song, T. Q., Wang, K. L., Yang, H., Yue, Y. M., Zeng, Z. X., Peng, W. X., and Zeng, F. P.:
892 Influences of stand characteristics and environmental factors on forest biomass and root-shoot
893 allocation in southwest China, *Ecol Eng*, 91, 7-15, 10.1016/j.ecoleng.2016.01.040, 2016.

894 Zhu, Z. C., Piao, S. L., Myneni, R. B., Huang, M. T., Zeng, Z. Z., Canadell, J. G., Ciais, P., Sitch, S.,
895 Friedlingstein, P., Arneeth, A., Cao, C. X., Cheng, L., Kato, E., Koven, C., Li, Y., Lian, X., Liu, Y.
896 W., Liu, R. G., Mao, J. F., Pan, Y. Z., Peng, S. S., Penuelas, J., Poulter, B., Pugh, T. A. M., Stocker,
897 B. D., Viovy, N., Wang, X. H., Wang, Y. P., Xiao, Z. Q., Yang, H., Zaehle, S., and Zeng, N.:
898 Greening of the Earth and its drivers, *Nat Clim Change*, 6, 791+, 10.1038/Nclimate3004, 2016.